

Review of Discrete X-Ray Sources in the Small Magellanic Cloud: Summary of the ASCA Results and Implication on the Recent Star-Forming Activity

Jun YOKOGAWA, Kensuke IMANISHI, Masahiro TSUJIMOTO, Katsuji KOYAMA

Department of Physics, Graduate School of Science, Kyoto University, Sakyo-ku, Kyoto 606-8502

jun@cr.scphys.kyoto-u.ac.jp

kensuke@cr.scphys.kyoto-u.ac.jp

tsujimot@cr.scphys.kyoto-u.ac.jp

koyama@cr.scphys.kyoto-u.ac.jp

and

Mamiko NISHIUCHI

Japan Atomic Energy Research Institute, Kansai Research Establishment,

8-1 Umebi-dai, Kizu-cho, Soraku-gun, Kyoto 619-0215

nishiuchi@apr.jaeri.go.jp

(Received 2002 June 24; accepted 2002 December 4)

Abstract

We made 22 observations on the Small Magellanic Cloud (SMC) and covered full regions of the main body and the eastern wing by the end of the ASCA mission. We detected 106 discrete sources with a criterion of $S/N > 5$ and performed systematic analyses on all of the sources. We determined the source positions with an $\sim 40''$ error radius (90% confidence) for sources detected in the central $20'$ radius of the GIS. We detected coherent pulsations from 17 sources. Among them, eight were newly discovered during this study. We classified most of these pulsars as X-ray binary pulsars (XBPs) based on their properties, such as the flux variability and the existence of an optical counterpart. We detected X-ray emission from eight supernova remnants (SNRs). Among them, five SNRs showed emission lines in their spectra, hence we regarded the five as thermal SNRs. We found that XBPs and thermal SNRs in the SMC can be clearly separated by their spectral hardness ratio. Applying this empirical law to faint (thus unclassified) sources, we found 19 XBP candidates and four thermal SNR candidates. We also found several tens of candidates for active galactic nuclei, both from the hardness ratio and the $\log N$ – $\log S$ relation of extragalactic sources. Based on these ASCA results and further information from ROSAT, SAX, RXTE, CGRO, Chandra, and XMM-Newton, we compiled comprehensive catalogues of discrete X-ray sources in the Small Magellanic Cloud. Using the catalogues, we

derived the spatial distributions of XBPs and SNRs. XBPs and SNRs were found to be concentrated in the main body and eastern wing, which resembles the distribution of young stars with ages of $\sim 2 \times 10^7$ yr. By comparing the source populations in the SMC and our Galaxy, we suggest that the star-forming rate (per unit mass) in the SMC was much higher than the Galaxy $\sim 10^7$ yr ago. We also discuss the recent change of the star-forming rate in the SMC.

Key words: galaxies: evolution — galaxies: individual (SMC, LMC) — galaxies: starburst — pulsars: general — source population study — X-rays: stars

1. Introduction

Depending on the mass (M) and the existence of a companion, stars evolve with different sequences, come to deaths, and leave various remnants. Binary systems of low-mass stars ($M \lesssim 8M_\odot$) evolve through an accreting white dwarf and type-Ia supernovae (SNe), and make the remnants (SNRs) within $\sim 10^9$ yr (Yoshii et al. 1996). Massive stars ($8M_\odot \lesssim M \lesssim 40M_\odot$), either single or binary, evolve more rapidly and come to type-II SNe, and leave SNRs within some 10^7 yr (in this paper we designate all non-type-Ia SNe as type-II), leaving neutron stars (NSs). Crab-like pulsars or high-mass X-ray binaries (HMXBs) are the remnants of single or binary massive stars, respectively. More massive stars leave black holes (BHs) within some 10^6 yr. Although the formation mechanisms of low-mass X-ray binaries (LMXBs) are still in dispute, NSs in LMXBs and their companion stars belong to old populations with ages of $\gtrsim 10^{8-9}$ yr. The remnants of stars, i.e., supernova remnants from type-Ia and type-II SNe (hereafter, type-Ia SNRs and type-II SNRs, respectively), young SNRs, Crab-like pulsars, HMXBs, LMXBs, and BH binaries comprise the brightest X-ray sources in a galaxy with a luminosity of $\gtrsim 10^{35}$ erg s $^{-1}$. Therefore, bright X-ray sources in a galaxy carry much information on the past star-forming activity, such as the rate and the site of star formation, mass function, and binary frequency.

Each class of the stellar remnants distinguishes itself by the X-ray spectrum and the temporal behaviour. Since X-ray emission from SNRs is mainly attributable to a shock-heated plasma, their spectra are relatively soft ($\lesssim 2$ keV) and dominated by emission lines from highly ionized atoms. The compositions of the atomic species produced by SNe depend on the types: light elements such as O, Ne, and Mg are mainly ejected from type-II SNe, while heavier elements such as Si, S, Ar, Ca, and Fe come from type-Ia SNe. Sources in the other classes have harder spectra than SNRs, showing a significant flux even at energies $\gtrsim 10$ keV. LMXBs have characteristic spectra which can be represented by a two-component thermal model (Mitsuda et al. 1984). Some of them occasionally exhibit X-ray bursts. BH binaries experience spectral transitions between the high-soft and low-hard states. Crab-like pulsars exhibit coherent pulsations with a short period ($\lesssim 1$ s) and a monotonous increase of the spin period (except for glitches). HMXBs have the hardest spectra, and exhibit long-term flux variations with a factor

of $\gtrsim 10$. Many HMXBs exhibit coherent pulsations with a long period ($\gtrsim 1$ s), and are thus classified as X-ray binary pulsars (XBPs). The ASCA satellite (Tanaka et al. 1994), with a reasonable energy resolution and high sensitivity for hard X-rays (> 2 keV) and a fine timing resolution, had a capability to distinguish the above-mentioned variety of X-ray properties, and to classify the X-ray source populations.

The Small Magellanic Cloud (SMC), a satellite of our Galaxy, is the next-nearest neighbor after the Large Magellanic Cloud (LMC). The proximity (60 kpc is assumed in this paper; van den Bergh 2000), reasonable angular size ($\sim 3^\circ \times 3^\circ$), and low interstellar absorption in the direction of the SMC are all favorable for an unbiased survey of the X-ray source populations covering the entire galaxy. Surveys of soft X-ray sources (below ~ 2 keV) have been carried out with the Einstein and ROSAT satellites (Wang, Wu 1992; Haberl et al. 2000; Sasaki et al. 2000). Haberl et al. (2000) present the most complete catalogue, which contains 517 ROSAT PSPC (Position Sensitive Proportional Counter) sources. Sasaki et al. (2000) used ROSAT HRI (High Resolution Imager) to determine the most accurate positions of 121 sources.

A hard X-ray study with ASCA in our earlier survey (Yokogawa et al. 2000e) classified many new sources into XBPs and thermal SNRs, and provided a simple (but reliable) method for this classification. However, because the ASCA survey did not cover all of the SMC fields, it may have had some bias for the population and distribution study.

After this early study, we have carried out new ASCA observations, and we have now covered the entire region of the SMC. This paper reports on the summary with particular emphasis on the ASCA new results. However, for completeness, we also extend to all the ASCA results as well as to some related results from ROSAT, SAX, RXTE, CGRO, Chandra, and XMM-Newton. Observation fields and the method of data reduction are presented in section 2. Source detection and position determination are described in section 3; the positional accuracy is discussed in detail. Timing and spectral analyses are performed for all sources as described in section 4. Comments on X-ray pulsars and SNRs are presented in section 5. Pulsar statistics, source classifications, source populations, and spatial distributions are discussed in section 6.

2. Observations and Data Reduction

ASCA observed the 22 SMC regions by the end of the mission, as summarized in table 1. Although the observations made before 1999 aimed at specific objects such as SNRs, X-ray pulsars, and a supersoft X-ray source, the assembly of these observations had already covered most of the main body and the eastern wing of the SMC. Our earlier study (Yokogawa et al. 2000e) is based on these observation data (except for obs. J). In order to cover all of the blank area, a survey project (SMC 1–10 in table 1) including long-exposure observations (SMC SW N1 and N2 in table 1) was performed. These observations covered most of the SMC region, as shown in figure 1. In this study, we used all of these observation data and carried out various analyses in a coherent manner.

In each observation, X-ray photons were collected with four XRTs (X-Ray Telescopes; Serlemitsos et al. 1995) and detected separately with two GISs (Gas Imaging Spectrometers; Ohashi et al. 1996) and two SISs (Solidstate Imaging Spectrometers; Burke et al. 1994). We rejected any data obtained in the South Atlantic Anomaly, or when the cut-off rigidity was lower than 4 GV, or when the elevation angle was lower than 5° . Particle events in the GIS data were removed by the rise-time discrimination method. SIS data obtained when the elevation angle from the bright Earth was lower than 25° , or with hot and/or flickering pixels, were also rejected. The effects of RDD (Residual Dark Distribution) on the SIS data were corrected with the method given in Dotani et al. (1997) for observations carried out later than 1996. After the screening, the total available exposure time for two GISs was ~ 2000 ks.

In order to uniformly study X-ray source populations, the GIS is more suitable than the SIS because of its larger field of view, larger effective area at high energy, and better time resolution. Therefore, we mainly used the GIS data in this study, while the SIS data were used for peculiar objects which need better energy resolution and/or better spatial resolution.

3. Source Catalogue

3.1. X-ray Images

Images in each observation were constructed in the sky and detector coordinate systems (hereafter “sky images” and “detector images”, respectively), with the XSELECT package. In the sky image, the position of each photon is determined using the instantaneous satellite attitude at the *incident time* of each photon. Therefore, the sky image is properly corrected for the image blurring due to attitude flickering. The data processing for the sky image is, however, limited to the photons coming within $\sim 20'$ radius on the GIS center. In the detector image, photons are accumulated in the coordinates fixed to each detector, and are then converted to the sky coordinates using the *average* attitude of the satellite during the observation. This software technique can be applied to a larger FOV of $\sim 25'$ in radius. We properly used the two different images: the sky images for sources within the central $\sim 20'$ radius (hereafter “inner circle”), and the detector images for the concentric region of $\sim 20'$ – $25'$ (hereafter “outer ring”). The outer ring region has a higher background, larger calibration error and distortion of the PSF than the inner circle region. For SIS, we always used sky images.

Figure 2 shows the GIS mosaic images in the soft (0.7–2.0 keV) and hard (2.0–7.0 keV) bands, created according to the method developed by Sakano (2000). A color-coded image in which soft and hard photons are indicated by red and blue is given in figure 3. In the color image, many hard sources and a few soft sources are clearly found.

3.2. Source Detection

For each observation, X-ray sources were extracted from images in the soft (0.7–2.0 keV), hard (2.0–7.0 keV), and total (0.7–7.0 keV) bands. We smoothed the images with a Gaussian

filter ($\sigma = 30''$), and examined the significance of each local peak (source candidate) found in the images as follows. Photons were extracted from a circle of $3'$ radius centered on the peak, in which 90% of the incident photons were contained (Serlemitsos et al. 1995), or from an ellipse at larger off-axis angles because of the distortion of the PSF. In several cases, a smaller circle/ellipse was used to avoid contamination from nearby peaks. For observation J, a larger circle was used, because in this observation the spatial resolution was reduced by a factor of 4, and thus the images were blurred. These photon events were also used in subsequent analyses described in the following subsections. Background regions were selected from the sky near each peak. We then derived the S/N, defined as $S/N \equiv [n(P) - n(B)]/\sqrt{n(B)}$, where $n(P)$ and $n(B)$ represent the photon counts in the circle/ellipse at the peak and in the background region, respectively. The local peak was identified as an X-ray source if the S/N ratio exceeded 5 in at least one of the soft-, hard-, or total-band images. In all, we detected 106 sources, of which 21 were detected in multiple observations (subsubsection 3.3.2).

In observation Q, sources No. 26 and No. 27 were resolved only in the SIS image with a separation of $\sim 1'.3$. No. 85 was detected only in the hard band because of severe contamination from No. 81 in the soft band. No. 88 and No. 89 are located near the calibration isotope of GIS 3; we thus used only GIS 2 to estimate the significance. Since No. 88 and No. 89 are separated by only $\sim 1'.5$, which caused severe mutual contamination, we used very small circles to estimate their S/N ratio. We found that the S/N of No. 89 well exceeds 5, while that of No. 88 is slightly less than 5. However, a local peak at No. 88 was also found evidently in GIS 3 (although no quantitative estimation is possible); we thus regard No. 88 as an X-ray source.

3.3. Position Determination

3.3.1. Absolute accuracy of the position

We first determined the position of each source simply by the coordinates of the peak pixel in the smoothed GIS images, and then performed a correction developed by Gotthelf et al. (2000). This correction compensates for the positional uncertainty caused by the ASCA attitude error, which depends on the temperature of the base-plate of the star-tracker and the geometry of the solar illumination. SIS images were used only for resolving sources No. 26 and No. 27 in obs. Q. According to this correction, the coordinates of some X-ray pulsars with “AX J” names (which have been included in previous publications) are now inconsistent with the source name; for example, the coordinates of No. 40 = AX J0051.6–7311 (Yokogawa et al. 2000b) are now ($00^{\text{h}}51^{\text{m}}44^{\text{s}}.5$, $-73^{\circ}10'34''$). In this paper, we do not rename these sources to avoid name confusion, and adopt the names used in the first publications for each pulsar.

This correction reduces the systematic positional uncertainty to $24''$ (90% error radius) for sources detected in the central $10'$ radius of the GIS (Gotthelf et al. 2000). However, additional errors from the photon statistics and the method of position determination, and errors for the sources located out of the central $10'$ radius, are unknown. Therefore, we examined

the “practical” errors for sources detected anywhere in the GIS as follows.

So far, the ROSAT HRI catalogue (Sasaki et al. 2000) presents the most accurate positions for the SMC X-ray sources, with an error radius of $\sim 1''$ – $10''$. Several sources in the ROSAT PSPC catalogue (Haberl et al. 2000) also have a small error radius of $\lesssim 10''$. Therefore, we investigated the separation angles between the ROSAT sources and their ASCA counterparts, which would represent the “practical” errors for the ASCA sources.

We primarily selected ASCA counterparts for the ROSAT sources that were within $90''$ of each ROSAT source. In order to reject accidental coincidences and ambiguous counterparts, we further employed spectral and temporal information of these sources as follows: (1) For sources catalogued in both the PSPC and HRI catalogues, only HRI sources were used, which provide more accurate positions. (2) Only ROSAT sources with an error radius smaller than $7''$ were used. Since the error radii for ASCA sources are $> 24''$, the additional error from the ROSAT sources is $< 1''$ when we take a root-sum square of all the errors. (3) For a ROSAT source with a Be star or a supergiant companion, the ASCA counterpart should exhibit coherent pulsations with a period of $\gtrsim 1$ s. The procedure for pulse detection is described in subsection 4.1. This criterion selects well-established XBPs. Although ASCA source No. 94 in obs. C exhibited no significant pulsations, it entered an eclipse phase as the ephemeris predicts for SMC X-1 (Wojdowski et al. 1998), thus we regard No. 94 in obs. C as SMC X-1. (4) For a ROSAT source at the position of a radio SNR, the ASCA counterpart should exhibit a soft spectrum with emission lines from ionized atoms. The method used to detect emission lines is described in subsection 4.2.3. This criterion selects bright thermal SNRs.

According to these criteria, we selected 19 pairs of ASCA–ROSAT counterparts, as summarized in table 2. Although No. 67 is certainly the counterpart for RX J0059.2–7138 (see subsection 5.1.16), this pair is not included in table 2 because No. 67 is detected at the very edge of the GIS (or may be slightly outside of the GIS) and so the position determination is not reliable. We show the separation angles as a function of the off-axis angle of the ASCA source in figure 4. No clear correlation between the separation angle and the off-axis angle could be found. Out of 17 ASCA sources detected in the inner circle (off-axis $< 20'$), 15 sources have separation angles less than $40''$. Therefore, we tentatively conclude that the “practical” error radius for GIS sources detected in the inner circle is $40''$ at 90% confidence level, although the statistics are rather limited. This is similar to the result obtained from the more elaborate analysis by Ueda et al. (1999). For sources detected in the outer ring, no constraint could be obtained due to the paucity of sources.

From the ROSAT and Einstein catalogues (Haberl et al. 2000; Sasaki et al. 2000; Wang, Wu 1992), we selected the counterpart for each ASCA source within a circle of a radius $\sim 60''$ for sources detected in the inner circle, or within a circle of a radius $\sim 70''$ for sources detected in the the outer ring. Radii larger than the 90% error radius ($40''$) were used in order to simply avoid missing identification.

3.3.2. Identification of sources detected in multiple ASCA observations

As shown in figure 1, neighbouring ASCA observation fields more or less overlap each other. Therefore, a pair of detections found in two observations within the overlapped region may be from the same source. In order to examine whether these pairs are the same source or not, we primarily selected pairs of detections within $90''$ of each other, and classified them into four classes (a)–(d) as follows: (a) Both of the sources exhibit coherent pulsations with nearly the same period, or exhibit emission lines from the same elements and have the same radio SNR as a counterpart (see subsection 4.1 and subsection 4.2.3 for the relevant analyses). (b) Both of the sources have soft spectra and have the same radio SNR as a counterpart. Pairs of No. 94 in obs. A and C and that in obs. I and C (SMC X-1) are also included in this class. Classes (a) and (b) surely consist of pairs of XBPs and thermal SNRs. (c) Both of the sources are located near the same pulsar and their spectral parameters are consistent with those of the pulsar. Sources of class (c) are likely to be X-ray pulsars. (d) The remainder.

We regarded detections in classes (a)–(c) as being from the same source, i.e., sources detected in multiple observations, and thus labeled them with the same source number in the ASCA catalogues (tables 5 and 6). We summarize the separation angle and the off-axis angles of classes (a)–(c) in table 3, while in figure 5 we give a plot of the separation angle vs. the larger off-axis angle. We found that the separation angle is $\lesssim 60''$ if both of the two sources are detected in the inner circle, or $< 73''$ if at least one of the two is detected in the outer ring. Therefore, we regard pairs of detections in class (d) to be the same source if they satisfy the above condition, and labeled them the same source number. Pairs thus selected are also summarized in table 3 and plotted in figure 5. After this selection, we concluded that ASCA detected 106 sources with no double count.

4. Analyses on Discrete Sources

In order to examine the nature of each source, we performed timing and spectral analyses in a coherent manner. The procedure of the analyses is essentially identical to that in Yokogawa et al. (2000e).

4.1. Timing Analyses

We performed a Fast Fourier Transform (FFT) analysis on all of the sources to search for coherent pulsations. At first, for sources with high count rates, we used only high-bit rate data in order to utilize the maximum time resolution (up to 62.5 ms). We then used high-bit and medium-bit data simultaneously for all sources, in order to achieve better statistics at the sacrifice of the time resolution to 0.5 s (7.8125 ms for obs. J and 125 ms for obs. O; see the caption of table 1). We detected coherent pulsations from 17 sources, eight of which are new discoveries from this study. Examples of the power spectrum densities (PSDs) are already shown in figure 2 of Yokogawa et al. (2000e) or chapter 5 of Yokogawa (2002). The detection

of pulses from No. 26 (AX J0049–732) and No. 83 (AX J0105–722) was not straightforward because of contamination from nearby sources. The details are described in subsection 5.1.4 and subsection 5.1.20, respectively.

In any observation, photon events were originally counted with a time spacing of 1/16 of the nominal resolution and stored in temporary memory. The events were then collectively sent to the telemetry with a time spacing equal to the nominal resolution. Therefore, if the event rate was so low as not to fill the memory, the time resolution could be 1/16 of the nominal value (Hirayama et al. 1996). For this reason, we carried out FFT analysis on several faint sources with a time resolution of 31.25 ms, using the high- and medium-bit data. The 87 ms pulsations from AX J0043–737 were thus discovered (see subsection 5.1.1 for further details).

In order to determine the pulse period precisely, we performed an epoch folding search for the 17 sources from which pulsations were detected by FFT analysis. The orbital Doppler effect was corrected only for SMC X-1, using the ephemeris presented by Wojdowski et al. (1998). The derived pulse periods are presented in table 4.

We detected no pulsations by FFT analysis from three sources that are positionally coincident with known pulsars: No. 43 (RX J0052.1–7319), No. 51 (XTE J0055–724), No. 74 (RX J0101.3–7211), and No. 94 in obs. C (SMC X-1). Therefore, we performed an epoch folding search around the known periods. Since SMC X-1 was in the 0.6-d eclipse phase during obs. C, we only used the data from the noneclipse times. Consequently, we detected a weak peak only from No. 51 at the known period of ~ 59 s, which is the evidence that No. 51 and XTE J0055–724 are the same source. This period is, however, not presented in table 4 because of the low significance of the pulse detection.

We also searched for burst-like activities by using light curves binned with various time scales from ~ 1 s to ~ 1 hr. Although no source exhibited bursts typical of LMXBs, No. 20 (RX J0047.3–7312 = IKT1, in obs. Q) showed a flare with a decay time of $\sim 2 \times 10^4$ s. Details are given in subsection 5.1.2.

4.2. Spectral Analyses

4.2.1. Overview

We analyzed the spectrum of each source and derived various parameters, as given in table 6: the hardness ratio (HR), photon index (Γ), temperature (kT), column density (N_{H}), flux (F_{X}), and absorption-corrected luminosity (L_{X}).

The analyses were not performed for No. 85, No. 88, and No. 89 because of severe contamination of these sources (see subsection 3.2). Spectra from GIS 2 and GIS 3 were co-added to increase the statistics, except for sources detected near the calibration isotope of either GIS and sources detected in only a single GIS¹. SIS spectra (SIS 0 + SIS 1) were used for No.

¹ Since the FOVs of the two GISs are pointed toward slightly different directions, it is possible for a source to be located at the very edge of one GIS and outside of the other GIS.

26 and No. 27 in obs. Q in order to spatially resolve these sources, and for SNRs 0045–734 (No. 21), 0047–735 (No. 25), 0057–7226 (No. 66), 0102–723 (No. 81), and 0103–726 (No. 82) to perform high resolution spectroscopy².

The parameters were derived by fitting the spectra with spectral models: different models were used according to the nature of each source, as described in subsections 4.2.3, 4.2.4, and 4.2.5. For sources detected in multiple observations (table 3), we first fitted the spectrum from each observation separately. Except for SMC X-1, the spectral parameters (Γ , kT , and N_{H}) in each observation were found to be consistent with each other. We thus simultaneously fitted all of the spectra with parameters linked between the observations, in order to obtain more stringent constraints. However, the flux was not linked in the simultaneous fitting, in order to examine the flux variability (readers should note that there could be $\lesssim 10\text{--}20\%$ error in the flux of most sources). Hardness ratios for those sources were derived after adding the spectra from all observations.

4.2.2. Hardness ratio

The spectral hardness ratio (HR) was derived by the definition $\text{HR} = (H - S)/(H + S)$, where H and S represent background-subtracted GIS count rates in 2.0–7.0 keV and 0.7–2.0 keV, respectively. HR is not given for No. 27 in table 6 because this source was only resolved with SIS (in obs. Q). For the same reason, HR of No. 26 was derived only from the data of obs. F.

4.2.3. Spectra of SNRs

X-rays were detected from the positions of eight radio SNRs³, 0045–734 (No. 21), 0047–735 (No. 25), 0057–7226 (No. 66), 0102–723 (No. 81), 0103–726 (No. 82), 0046–735 (No. 23), 0049–736 (No. 36), and 0056–725 (No. 64). The former five were detected with SIS and the latter three were detected only with GIS. At first, we investigated the presence of emission lines in the spectra with the same method described in subsection 3.4 of Yokogawa et al. (2000e). We found evidence of emission lines from 0045–734, 0057–7226, 0102–723, 0103–726, and 0049–736, and thus we regard these five as thermal SNRs. We therefore fitted their spectra with thin-thermal plasma models, as described in subsection 5.2. For the other SNRs, we first fitted the spectra with both a power-law model and a thin-thermal model in a collisional ionization equilibrium (CIE) state (Raymond, Smith 1977), and finally adopted a power-law for 0056–725 and the CIE thermal model for 0047–735 and 0046–735, for reasons described in subsection 5.2. When fitting with thermal models, the metal abundances were primarily fixed at 0.2 solar, which is the mean value for the SMC ISM (Russell, Dopita 1992),

² For 0047–735, the SIS spectrum in obs. F was not used because the statistics were too poor.

³ No. 83 (AX J0105–722) was once identified with SNR DEM S128 (Yokogawa et al. 2000e), but now the identification is questionable due to the improved position of the ASCA source and the high resolution ROSAT study (Filipović et al. 2000a). See also subsection 5.1.20.

unless otherwise mentioned. Hereafter, we refer to this abundance value as “the SMC abundance.”

4.2.4. Spectra of X-ray pulsars and HMXBs

The spectra of X-ray pulsars (regardless of whether they are accretion-powered or rotation-powered) are generally described by a power-law in the ASCA bandpass. Therefore, we adopted a power-law model for the 22 detected pulsars (summarized in table 4) and also for No. 63 (a Be/X-ray binary, RX J0058.2–7231).

Several sources exhibited systematic deviation from the simple power-law. Since No. 49 (SMC X-2) and No. 90 (XTE J0111.2–7317) showed bump-like residuals around 6–7 keV, we added a narrow Gaussian line to the model. For No. 67 (RX J0059.2–7138), the power-law model exceeded the data at $\gtrsim 7$ keV, and thus we included a high-energy cutoff in the model. The brightest pulsars (RX J0059.2–7138, XTE J0111.2–7317, and SMC X-1) all exhibited large data excess over the power-law at $\lesssim 2$ keV, thus we added a blackbody component to describe the soft excess. Details of the analyses and comments are given for each source in subsection 5.1.

4.2.5. Remaining sources

Although the nature of X-ray emission from the remaining sources is unclear at this moment, we basically adopted a power-law model in the spectral fitting. Since No. 22 (AX J0048.2–7309) showed weak evidence for an emission line at around 6–7 keV, we added a Gaussian line to the model (see subsection 5.3.1). For No. 2 and No. 13, no constraint on the spectral parameters could be obtained due to the highly limited statistics; we thus do not present the parameters in table 6. For No. 39, the best-fit model ($\Gamma = 10$ and $N_{\text{H}} = 1.4 \times 10^{23} \text{ cm}^{-2}$) yielded a very high luminosity of $L_{\text{X}} \sim 3 \times 10^{39} \text{ erg s}^{-1}$. Such a high luminosity is unrealistic and is probably an artifact caused by the large Γ and N_{H} ; we thus do not present L_{X} in table 6. For very soft sources (No. 6 and No. 45), we present the results from both a power-law model and a CIE thermal model.

5. Comments on Specific Sources

5.1. X-Ray Pulsars

Since the first X-ray pulsar in the SMC, SMC X-1, was discovered (Lucke et al. 1976), only three pulsars had been known for about 20 years (Hughes 1994; Israel et al. 1997). In the last four years, however, there has been a rush of pulsar discoveries (see figure 6), and now there are 30 pulsars known in the SMC (table 4).

In this subsection, we give brief comments on all of the X-ray pulsars in order to summarize their nature. Since no new information has been obtained for XTE J0055–724, 2E 0050.1–7247, and RX J0117.6–7330, we give the same comments as described in Yokogawa

et al. (2000e). The pulse periods are designated with the error for the last digit in parentheses. We regarded a pulsar as an XBP if the pulsar had a long pulse period ($\sim 1\text{--}1000$ s), hard spectrum ($\Gamma \sim 1$), flux variability, and/or an optical counterpart. Finally we classified 26 out of the 30 pulsars as XBPs. The spectra and pulse shapes are given in the references for each pulsar, and are also summarized in Yokogawa (2002).

5.1.1. No. 17 — AX J0043–737

Coherent pulsations of a 87.58073(4) ms period from AX J0043–737 were discovered by Yokogawa and Koyama (2000) in obs. K, using a timing resolution of 31.25 ms (1/16 of the nominal value) as described in subsection 4.1. The significance of the detection is at a marginal level, $\sim 99.98\%$. AX J0043–737 was also detected in a follow-up observation with a longer exposure time (obs. P). Although we performed the FFT on the events in the same energy band, no significant peak was found. The count rate, total count (without background), and background level in 0.5–7.7 keV are 2.5×10^{-3} count s $^{-1}$, 200 count, and 64% in obs. K, and 1.0×10^{-3} count s $^{-1}$, 186 count, and 84% in obs. P. Although the total count is nearly identical in these two observations, the smaller count rate and larger background level in obs. P may have caused the pulsations to be hidden in the background. Therefore, a confirmation of the pulsations by observations with much higher S/N ratios is still needed.

The spectral shape (Γ and N_{H}) is consistent between the two observations, while F_{X} shows a slight decline (table 6). The photon index (~ 1.7) is softer than those for usual XBPs, $\Gamma \sim 1$ (e.g., Nagase 1989). A short pulse period, soft spectrum, and luminosity far smaller than the Eddington limit for a neutron star are also detected from SAX J0635+0533 ($P = 33.8$ ms and $\Gamma = 1.50$), which has a Be star counterpart (Kaaret et al. 1999; Cusumano et al. 2000). Cusumano et al. (2000) argued that SAX J0635+0533 may be an accretion-powered Be/X-ray binary, and if so, the magnetic field should be weaker than 2×10^9 G for the accretion to occur against the centrifugal force at the magnetosphere.

Since no optical counterpart has been reported for AX J0043–737, we investigated the catalogues of emission-line objects (potential candidates for Be stars) by Meyssonier and Azzopardi (1993) and Murphy and Bessell (2000), but no counterpart was found. Therefore, a search for the optical counterpart is needed, in addition to confirmation of the 87-ms pulsations.

5.1.2. No. 20 — RX J0047.3–7312 = IKT1

We tentatively consider No. 20, RX J0047.3–7312, and IKT1 to be identical simply because of the positional coincidence. Haberl and Sasaki (2000) proposed RX J0047.3–7312 as a Be/X-ray binary candidate because this source exhibits a flux variation with a factor of 9 and has an emission-line object as a counterpart. The GIS spectra in two observations (F and Q) are hard, having a photon index of ~ 1 , which is typical of Be/X-ray binaries. In addition, a flare-like behaviour was found from the light curve in obs. Q (figure 8).

Archival data from an XMM-Newton observation revealed that this source is pulsating

with a period of 263(1) s (M. Ueno, private communication). All of these results indicate that RX J0047.3–7312 is probably an XBP with a Be star companion (hereafter, a Be-XBP).

5.1.3. No. 24 — AX J0049–729

Corbet et al. (1998), using RXTE, first discovered pulsations with a 74.8(4) s period in the direction of SMC X-3, with a large positional uncertainty of $\sim 2^\circ$. During this study, we found that AX J0049–729 was pulsating with a 74.68(2) s period in obs. F (Yokogawa et al. 1999). The position was determined more accurately and is consistent with the 74.8-s pulsar discovered with RXTE. The ROSAT counterpart of this pulsar, RX J0049.1–7250, provides the most accurate position with a $\pm 13''$ error circle (Kahabka, Pietsch 1998), in which one Be star has been discovered (Stevens et al. 1999). Yokogawa et al. (1999) found a large flux variability with a factor of $\gtrsim 100$ using archival data of Einstein and ROSAT. From all of the information, we conclude that AX J0049–729 is a Be-XBP.

5.1.4. No. 26 — AX J0049–732

Coherent pulsations with a 9.1320(4) s period from AX J0049–732 were first detected during this study in the following manner. Using the data of obs. F, we performed an FFT on the events in 1.0–5.1 keV collected from a $3'$ -radius circle centered on AX J0049–732, and discovered the coherent pulsations with 99.99% confidence (Imanishi et al. 1998; Ueno et al. 2000a). However, since AX J0049–732 was detected at only $\sim 1'.8$ from No. 25 (SNR 0047–735), mutual contamination was not negligible due to the poor resolution of the ASCA XRT. Therefore, we also performed an FFT on the events in a $3'$ -radius circle centered on SNR 0047–735, and detected no pulsations. These analyses clearly indicate that the 9.13-s pulsations are attributable to AX J0049–732.

AX J0049–732 was also detected in obs. Q. However, in this observation another source, No. 27, was detected at $\sim 1'.3$ from AX J0049–732, in addition to SNR 0047–735 at $\sim 1'.8$ apart. The SIS data were used to resolve these sources and determine the spectral parameters, but were not used for an FFT analysis because the timing resolution (8 s) is insufficient to detect the ~ 9 -s pulsations. We therefore used the GIS data for an FFT analysis, although No. 27 and AX J0049–732 were not resolved. We collected photons from a $3'$ -radius circle centered on AX J0049–732 and performed the FFT analysis, but no significant pulsations were detected. This was probably due to the poor statistics caused by the reduced flux of AX J0049–732 and large contamination from No. 27, which has the same flux level as AX J0049–732 (see table 6). Therefore, a follow-up observation with better spatial resolution is needed to confirm the pulsations from AX J0049–732.

Two ROSAT sources, RX J0049.2–7311 and RX J0049.5–7310 (No. 430 and No. 427 in Haberl et al. 2000, respectively), were found near AX J0049–732 (Filipović et al. 2000a). Since RX J0049.2–7311 has an emission-line object as a counterpart, while RX J0049.5–7310 does not, Filipović et al. (2000a) suggested that RX J0049.2–7311 is likely to be the counterpart

for AX J0049–732. However, according to the updated position of the ASCA source, the separation between AX J0049–732 and RX J0049.2–7311 is $\sim 80''$, which is much larger than the improved positional accuracy for ASCA sources (see subsection 3.3.1). Therefore, the identification made by Filipović et al. (2000a) is now questionable. On the other hand, the separation between RX J0049.5–7310 and AX J0049–732 is $\sim 33''$, thus we regard this source as the counterpart.

5.1.5. No. 30 — AX J0049.5–7323

Coherent pulsations with a 755.5(6) s period from AX J0049.5–7323 were first discovered during this study from the data of obs. Q (Ueno et al. 2000b; Yokogawa et al. 2000a). Yokogawa et al. (2000a) investigated the archival data of 19 observations of ROSAT and Einstein in which AX J0049.5–7323 was covered, and found a flux variation with a factor of at least ~ 10 . All of the information indicates that AX J0049.5–7323 is an XBP. In addition, the ROSAT counterpart, RX J0049.7–7323, is proposed to be a Be/X-ray binary because an emission-line object exists in the error circle of $\sim 15''$ -radius (Haberl, Sasaki 2000). An optical spectroscopy of the emission-line object is encouraged to examine whether it is a Be star or not.

5.1.6. No. 32 — AX J0051–733

Coherent pulsations with a 323.2(5) s period from AX J0051–733 were first discovered during this study from the data of obs. F and reported by Yokogawa and Koyama (1998a) and Imanishi et al. (1999). New results were obtained from a long follow-up observation (obs. Q): AX J0051–733 was detected at a larger flux (see table 6) and the pulsations were detected again with a shorter period of 321.0(1) s. Imanishi et al. (1999) investigated the archival data of 16 observations of ROSAT and Einstein in which AX J0051–733 was covered, and found a flux variability of a factor $\gtrsim 10$. In addition, a gradual flux increase with a factor of ~ 2 was found during obs. Q. The ROSAT counterpart, RX J0050.8–7316, has a Be star in its error circle (Cowley et al. 1997). All of this information indicates that AX J0051–733 is a Be-XBP.

From the empirical relation between the pulse and orbital periods of Be-XBPs (Corbet 1984), the orbital period of AX J0051–733 is predicted to be ~ 185 d. On the other hand, due to an optical photometric study of the Be star counterpart, strong evidence for a modulation with a 0.7-d period was found (Coe, Orosz 2000; Coe et al. 2002). Coe and Orosz (2000) argued that if the modulation is due to the orbital motion, the orbital period should be 1.4 d. The large discrepancy between Corbet’s empirical law and the period seen in the optical band is rather problematic, and must be solved by future studies.

5.1.7. No. 37 — AX J0051–722

Coherent pulsations with a ~ 92 s period were first discovered in the direction of SMC X-3 during an RXTE observation on 1997 November 15 (Marshall et al. 1997). A TOO (Target Of Opportunity) observation with ASCA on December 12 (obs. H) revealed that there were

two new pulsars, AX J0051–722 and 1WGA J0053.8–7226, with periods of 91.12(5) s and 46.63(4) s, respectively (Corbet et al. 1998). At first, AX J0051–722 steadily faded after its discovery, and then was found to rebrighten at the ends of March and July in 1998 (Lochner et al. 1998; Lochner 1998; Israel et al. 1998a). The spacing of these two flares and the initial outburst on 1997 November is ~ 120 d.

Stevens et al. (1999) carried out optical spectroscopic observations and discovered a Be star counterpart for AX J0051–722. Thus, AX J0051–722 is classified as a Be-XBP. Therefore, the ~ 120 -d spacing of X-ray flares could be interpreted as the orbital period of the neutron star in this system (Israel et al. 1998a), which is supported by the empirical law between the pulse and orbital periods (Corbet 1984).

5.1.8. No. 40 — AX J0051.6–7311

Coherent pulsations with a 172.40(3) s period from AX J0051.6–7311 were first discovered during this study from the data of obs. Q (Torii et al. 2000a; Yokogawa et al. 2000b). AX J0051.6–7311 has been covered by 17 observations of ROSAT and Einstein. Yokogawa et al. (2000b) investigated these archival data and found a flux variation with a factor of $\gtrsim 20$. In addition, the ROSAT counterpart, RX J0051.9–7311, has been identified with a Be star (Cowley et al. 1997). Therefore, all of the information indicates that AX J0051.6–7311 is a Be-XBP.

5.1.9. No. 43 — RX J0052.1–7319

Coherent pulsations with a 15.3 s period from RX J0052.1–7319 were discovered in contemporaneous ROSAT and CGRO observations in 1996 (Lamb et al. 1999). Kahabka (2000) investigated the data of two ROSAT HRI observations in 1995 and 1996 and found a large change of flux with a factor of ~ 200 . The unabsorbed luminosities in the ROSAT band were determined to be 2.6×10^{35} erg s $^{-1}$ and 5.2×10^{37} erg s $^{-1}$ (in 0.1–2.4 keV; P. Kahabka 2001, private communication), assuming a photon index of 1.0 and a column density of 3×10^{21} cm $^{-2}$. Israel et al. (1999) searched for an optical counterpart in the 10'' error circle and discovered a Be star, in addition to a fainter object with an unknown spectral type. From all of the information, RX J0052.1–7319 is thought to be a Be-XBP.

A faint ASCA source, No. 43, is positionally coincident with RX J0052.1–7319. The ASCA spectrum puts almost no constraint on the parameters (see table 6) and is consistent with Γ and N_{H} assumed by Kahabka (2000). We detected no sign of coherent pulsations from either an FFT analysis or an epoch folding search, which is probably due to the highly limited statistics. Therefore, it is not clear whether No. 43 is really the counterpart of RX J0052.1–7319.

5.1.10. No. 44 — XTE J0054–720

A transient pulsar XTE J0054–720, with a period of ~ 169 s, was discovered with RXTE (Lochner et al. 1998). A flux variation and a monotonous spin-up were found in the initial

RXTE observations. Since the RXTE error circle was rather large ($10'$ radius), identification with other sources has been difficult. In fact, five ROSAT HRI sources (Sasaki et al. 2000) are located within the error circle. During this study, we detected coherent pulsations with a 167.8(2) s period from No. 44 (AX J0052.9–7157) and determined its position accurately (Yokogawa et al. 2001a). We found that AX J0052.9–7157 is located within the error circle of XTE J0054–720 and has a variable Be/X-ray binary, RX J0052.9–7158 (Cowley et al. 1997), as a counterpart. From the nearly equal pulse period and the positional coincidence, we conclude that the ASCA, ROSAT, and RXTE sources are identical, and thus XTE J0054–720 is a Be-XBP.

5.1.11. No. 47 — 1WGA J0053.8–7226 = XTE J0053–724

Coherent pulsations from 1WGA J0053.8–7226 with a 46.63(4) s period were discovered in obs. H, as described in subsection 5.1.7 (Corbet et al. 1998). Buckley et al. (2001) investigated the archival data of 21 ROSAT observations, and found a large flux variability. They also carried out follow-up optical and infrared observations, and discovered two Be stars in the error circle. All of the information indicates that 1WGA J0053.8–7226 is a Be-XBP.

5.1.12. No. 49 — SMC X-2

SMC X-2 is a long-known transient Be/X-ray binary with a maximum luminosity of $\sim 10^{38}$ erg s $^{-1}$ (Clark et al. 1978; Murdin et al. 1979). Large outbursts have been detected with SAS-3, HEAO1, and ROSAT (Clark et al. 1978; Marshall et al. 1979; Kahabka, Pietsch 1996).

Corbet et al. (2001b) detected a large outburst ($\sim 10^{38}$ erg s $^{-1}$) in the direction of SMC X-2 in 2000 January–April, with the All-Sky Monitor onboard RXTE. The position was determined with an error radius of $3'$, and SMC X-2 is located near the edge of the error circle. Coherent pulsations were also discovered during the outburst, with periods of 2.371532(2) s on April 12 and 2.371861(3) s on April 22–23. We made a follow-up ASCA observation (obs. R) and detected No. 49 at the position consistent both with SMC X-2 and the 2.37-s pulsar. We also detected pulsations with a 2.37230(4) s period (Yokogawa et al. 2001b), which is in full agreement with the RXTE result, indicating that the RXTE pulsar and No. 49 are identical.

The emission line seen in the spectrum (subsection 4.2.4) has a center energy of 6.3 (6.1–6.5) keV, which is consistent with the K-shell emission from neutral or low-ionized Fe, and has an equivalent width of 400 (150–640) eV. Yokogawa et al. (2001b) carried out a pulse-phase-resolved spectroscopy, and found marginal evidence for pulsations of the Fe line intensity.

5.1.13. No. 51 — XTE J0055–724 = 1SAX J0054.9–7226

A scan observation made with RXTE on 1998 January 20 revealed a new X-ray pulsar, XTE J0055–724, with a pulse period of ~ 59 s (Marshall, Lochner 1998). Santangelo et al. (1998) made a follow-up observation with SAX on January 28, and detected pulsations with

a 58.963(3) s period from 1SAX J0054.9–7226, which is located within the 10′ error circle of XTE J0055–724. The agreement of the period and position indicates that XTE J0055–724 and 1SAX J0054.9–7226 are the same source. During this study, we detected weak evidence for ~ 59 s pulsations from No. 51, which is positionally coincident with 1SAX J0054.9–7226; hence, we consider No. 51 to be the counterpart for this pulsar.

Israel et al. (1998b) investigated the archival data of 13 ROSAT observations covering 1SAX J0054.9–7226. They found a flux variation with a factor of > 30 between two observations of ROSAT in 1996 and RXTE in 1998. They also determined the position with a 10″ error circle, in which a Be star was later discovered by Stevens et al. (1999). XTE J0055–724 = 1SAX J0054.9–7226 is thus a Be-XBP.

5.1.14. No. 56 — AX J0057.4–7325

Coherent pulsations with a 101.45(7) s period from AX J0057.4–7325 were first discovered during this study from the data of obs. R (Torii et al. 2000b; Yokogawa et al. 2000c). This source was also found in obs. L, and weak evidence for pulsations with a period of 101.47(6) s was detected. Yokogawa et al. (2000c) investigated six ROSAT observations covering this pulsar, and found a flux variability with a factor of > 10 . All of the information indicates that AX J0057.4–7325 is an XBP.

So far optical follow-up observations have not been carried out. As far as we have investigated, only one optical source, MACS J0057–734#010, is located within the ASCA error circle (Tucholke et al. 1996), for which the spectral type and existence of the H α emission line are not known. No counterpart is found in the catalogues of emission-line objects by Meyssonier and Azzopardi (1993) and Murphy and Bessell (2000). This is a rare case in which an XBP in the SMC is not associated with a Be star or an emission-line object (see Haberl, Sasaki 2000). We note that AX J0057.4–7325 is located at the edge of the SMC main body, fronting the eastern wing. The fact that OB supergiant X-ray binaries (only SMC X-1 and EXO 0114.6–7361; see tables 4 and 8) are both located in the eastern wing leads us to suspect that AX J0057.4–7325 might be the third example. Therefore, deep and detailed optical observations around this pulsar are strongly encouraged.

5.1.15. No. 61 — AX J0058–7203

Coherent pulsations with a period of 280.4(4) s from AX J0058–7203 were first discovered during this study (Yokogawa, Koyama 1998a; Tsujimoto et al. 1999). In a new observation T, AX J0058–7203 was detected at a large off-axis angle of $\sim 23'$. We performed an FFT analysis and found no significant pulsations. The count rate, total counts (without background), and background level in 1.0–6.0 keV are 1.3×10^{-2} count s $^{-1}$, 1014 count, and 39% in obs. G, and 7.3×10^{-3} count s $^{-1}$, 642 count, and 42% in obs. T. The reduced total counts may cause the non detection of pulsations, although no quantitative estimation has been done.

Tsujimoto et al. (1999) investigated archival data of 14 observations with Einstein and ROSAT covering this pulsar, and found a flux variation with a factor of $\gtrsim 10$. Haberl and Sasaki (2000) found an emission-line object as a counterpart for AX J0058–7203. All of this information indicates that AX J0058–7203 is an XBP, and probably has a Be star companion.

5.1.16. No. 67 — RX J0059.2–7138

A transient source, RX J0059.2–7138, was discovered with ROSAT and ASCA in simultaneous observations of SNR 0102–723 (obs. B). Coherent pulsations with a period of 2.7632(2) s were discovered from the ROSAT data (Hughes 1994), and were confirmed with the ASCA data (Kohno et al. 2000). The pulsed fraction is larger at higher energy (Hughes 1994; Kohno et al. 2000). The possible optical counterpart proposed by Hughes (1994) was later revealed to be a Be star (Southwell, Charles 1996), and thus RX J0059.2–7138 is undoubtedly a Be-XBP.

The ASCA spectrum exhibits a soft excess below $\lesssim 2$ keV and a cut-off above $\gtrsim 7$ keV, as described in subsection 4.2.4. We thus included a blackbody model as the soft component and a high-energy exponential cut-off. Kohno et al. (2000) used the ROSAT and ASCA data simultaneously, and carried out more elaborate analyses. They adopted various models to describe the soft excess, and found that the soft component could be described by a thin-thermal plasma model or a broken power-law combined with an oxygen overabundance in the absorption column. They also found that the normalization of the soft component does not change (i.e., the soft component exhibits no pulsations) during the pulse phase, which is consistent with the energy-dependent pulsed fraction.

5.1.17. No. 72 — CXOU J0110043.1–721134

Lamb et al. (2002b) carried out a 100-ks Chandra observation, and discovered coherent pulsations with a period of 5.44 s from CXOU J0110043.1–721134. Its spectrum was fitted by a blackbody model with a temperature of ~ 0.41 keV and a luminosity of $\sim 10^{35}$ erg s $^{-1}$. They investigated the archival data from other satellites, and found little flux variation. From all of the information, Lamb et al. (2002b) proposed that CXOU J0110043.1–721134 is an anomalous X-ray pulsar (AXP).

We found that the ASCA spectrum of No. 72, originally fitted by a soft power-law model ($\Gamma \sim 3$), could also be described by a blackbody model with a temperature of ~ 0.41 keV. This fact confirms that No. 72 is the counterpart for CXOU J0110043.1–721134.

5.1.18. No. 74 — RX J0101.3–7211

RX J0101.3–7211 has been known to be a highly variable ROSAT source with an emission-line object (Haberl, Sasaki 2000), and was classified as an XBP candidate in our earlier study (source No. 27 in Yokogawa et al. 2000e) because of its hard spectrum. Therefore, this source has been strongly suspected to be a Be-XBP, although no pulsations were detected,

probably because of the limited statistics.

Sasaki et al. (2001) analyzed an XMM-Newton observation on SNR 0102–723 and serendipitously detected RX J0101.3–7211. Although the flux level was the lowest among previous detections with ROSAT and ASCA, coherent pulsations with a 455(2) s period were discovered thanks to the high S/N ratio achieved by XMM-Newton. The pulsed fraction was found to be energy-dependent and higher at lower energy, the same as AX J0049.5–7323 (Ueno et al. 2000b). Sasaki et al. (2001) also carried out a spectroscopic optical observation on the emission-line object found by Haberl and Sasaki (2000), and revealed it to be a Be star. Therefore, RX J0101.3–7211 is undoubtedly a Be-XBP.

5.1.19. No. 78 — 1SAX J0103.2–7209

Hughes and Smith (1994) and Ye et al. (1995) performed ROSAT HRI observations of the shell-like radio SNR 0101–724 and detected no X-rays from the radio shell. Instead, an X-ray point source RX J0103.2–7209 (= 1SAX J0103.2–7209) having a Be star counterpart was detected inside the SNR.

Coherent pulsations with a period of 345.2(3) s from 1SAX J0103.2–7209 were first discovered in a SAX observation made on 1998 July 26–27 (Israel et al. 1998a, 2000). Subsequently, pulsations with a period of 348.9(3) s were detected from the ASCA source No. 78 on 1996 May 21–23, (obs. D; Yokogawa, Koyama 1998c). Israel et al. (2000) also detected 343.5(5) s pulsations from Chandra data obtained on 1999 August 23, and found a monotonous spin-up with a period derivative of -1.7 s yr^{-1} .

1SAX J0103.2–7209 has been detected in various observations with Einstein, ROSAT, ASCA, and Chandra, with nearly the same luminosity level of $\lesssim 10^{36} \text{ erg s}^{-1}$ (Israel et al. 2000, and references therein). According to this fact, Israel et al. (2000) argued that this pulsar can possibly be classified as a “persistent” Be-XBP, such as X Per, RX J0146.9+6121, RX J0440.9+4431, and RX J1037.5–564 (White et al. 1983; Mereghetti et al. 2000; Reig, Roche 1999). The 755-s pulsar AX J0049.5–7323 (subsection 5.1.5) may also belong to this class, although the upper limit of the flux variation is not known.

5.1.20. No. 83 — AX J0105–722

Since AX J0105–722 and No. 84 are located only $\sim 3'$ from each other, mutual contamination is not negligible. We therefore used an oval-shaped region including both AX J0105–722 and No. 84 (region 1 in figure 7a) in the timing analysis, and detected coherent pulsations with a 3.34300(3) s period at a marginal significance of $\sim 99.5\%$ (Yokogawa, Koyama 1998b). We then separately searched for pulsations from regions 2 and 3 in figure 7b and found weak evidence for the 3.34-s pulsations only from region 2 (which includes AX J0105–722). Therefore, we conclude that the pulsations are attributable to AX J0105–722. The spectrum of AX J0105–722 is rather soft (see table 6) compared to those of typical XBPs, $\Gamma \sim 1$ (Nagase 1989).

Filipović et al. (2000b) used the data from high resolution X-ray and radio observations around this source made with ROSAT, ATCA (Australia Telescope Compact Array), and MOST (Molonglo Observatory Synthesis Telescope). They resolved the ASCA sources AX J0105–722 and No. 84 into five ROSAT PSPC sources as shown in figure 7c: AX J0105–722 is surrounded by three ROSAT PSPC sources, Nos. 145, 147, and 163 (here, PSPC-145, PSPC-147, and PSPC-163) in Haberl et al. (2000). PSPC-163 (RX J0105.1–7211) exhibits a hard spectrum typical of HMXBs and is identified with an emission line object catalogued in Meyssonier and Azzopardi (1993), and thus is a likely candidate for a Be/X-ray binary (e.g., Haberl, Sasaki 2000). PSPC-145 is positionally coincident with the radio emission from SNR DEM S128, has a soft X-ray spectrum typical of SNRs, and exhibits no flux variation, and is thus likely to be an X-ray emitting SNR. PSPC-147 has the hardest spectrum among the three, although the source nature of the source is unclear. Considering these facts, we propose that the 3.34-s pulsations can be attributed to RX J0105.1–7211, which is a Be-XBP, and that the mutual contamination of X-rays from RX J0105.1–7211, PSPC-145, and PSPC-147 in the ASCA data caused the rather soft spectrum of AX J0105–722. Because of this situation and the rather marginal detection of pulsations, follow-up X-ray observations with high spatial resolution and good S/N ratio are needed.

5.1.21. No. 90 — XTE J0111.2–7317

A transient source, XTE J0111.2–7317, was serendipitously found with RXTE and CGRO, and at the same time coherent pulsations with a period of ~ 31 s were discovered (Chakrabarty et al. 1998a; Wilson, Finger 1998). In the TOO observation with ASCA (obs. I), pulsations with a 30.9497(4) s period were unambiguously detected from No. 90. Thus No. 90 is undoubtedly the counterpart for XTE J0111.2–7317, and the position was determined with an accuracy better than RXTE (Chakrabarty et al. 1998b). Israel et al. (1999) detected two stars in the error circle; the fainter one was revealed to be a Be star and was proposed to be the optical counterpart for this pulsar. Coe et al. (2000) carried out a more elaborate optical spectroscopy on the optical counterpart, and confirmed the Be nature of this star. Therefore, XTE J0111.2–7317 is undoubtedly a Be-XBP.

The soft X-ray excess shown in the spectrum was well fitted with a blackbody model (subsubsection 4.2.4). However, the pulse phase resolved spectroscopy performed by Yokogawa et al. (2000d) revealed that the blackbody component is pulsating, while the emission region of the blackbody is extremely large (~ 800 km in radius) and so pulsation is impossible. Therefore, Yokogawa et al. (2000d) proposed an alternative model, the “inversely broken power-law,” which is a power-law with a larger/smaller photon index below/above a break energy, to describe the whole continuum and the pulsations in the low energy band. The pulsations of the soft component are in striking contrast to the non-pulsating soft component of RX J0059.2–7138 (subsubsection 5.1.16), although the overall continuum shapes in the ASCA band resemble each

other.

5.1.22. *No. 94 — SMC X-1*

SMC X-1 is a well-established XBP with a pulse period of ~ 0.71 s, having a B-type supergiant companion (e.g., Bildsten et al. 1997). SMC X-1 has been detected in three ASCA observations. The 0.71-s pulsations were detected only from the data of obs. A and obs. I. In obs. C, it was in a low-state and went into eclipse as predicted by the ephemeris of Wojdowski et al. (1998). Since the low-state of SMC X-1 should be caused by an occultation of the X-ray emitter, probably by the tilted accretion disk (Wojdowski et al. 1998; Vrtilik et al. 2001), the intrinsic luminosity in the low-state should be as high as that in the high-state. Therefore, the small F_X and L_X derived from the obs. C data (table 6) appear to be an underestimate of the true intensity.

The soft excess, which was described by a blackbody component (subsubsection 4.2.4), was found to be pulsating by a phase-resolved spectroscopy performed on the obs. A data (Paul et al. 2002). Therefore, for the same reason as described in subsubsection 5.1.21, attributing the soft excess to blackbody emission is not appropriate. Paul et al. (2002) found that the inversely broken power-law model or two-component power-law model could describe both the continuum shape and the pulsating nature of the soft excess.

5.1.23. *XTE J0050–732#1 and #2*

Lamb et al. (2002a) discovered two new pulsars with periods of 16.6 s and 25.5 s from archival data of RXTE. Although they gave no names for these pulsars, we tentatively designate them as XTE J0050–732#1 (16.6 s) and XTE J0050–732#2 (25.5 s) because the RXTE observation was centered on ($00^{\text{h}}50^{\text{m}}44.^{\text{s}}64$, $-73^{\circ}16'04.''8$). From the long pulse periods and the period derivative (found only for XTE J0050–732#1), we regard both as XBPs, although more information (optical counterparts and flux variability) is required for a further confirmation.

5.1.24. *2E 0050.1–7247*

Coherent pulsations with a 8.8816(2) s period from 2E 0050.1–7247 = RX J0051.8–7231 were discovered in a ROSAT observation by Israel et al. (1997). A flux variability with a factor 20 between two ROSAT observations and a Be star in the error circle were found; hence, this pulsar is a Be-XBP. ASCA covered the position of 2E 0050.1–7247 in obs. H. We did not detect any positive excess above the background level from this position. The upper limit of its flux is estimated to be $\sim 1 \times 10^{-13} \text{erg s}^{-1} \text{cm}^{-2}$ (0.7–10.0 keV), assuming a photon index of ~ 1 .

5.1.25. *XTE J0052–723*

A new transient pulsar XTE J0052–723 with a period of 4.782(1) s and a flux of 8 mCrab was discovered with RXTE (Corbet et al. 2001a). The pulse period indicates that this source is an XBP, probably a Be-XBP because of the transient nature. The position was determined

with a $2' \times 1'$ error box, and is covered by ASCA observation H. We detected no X-rays from this position, and set the upper limit to be $\sim 1 \times 10^{-13} \text{erg s}^{-1} \text{cm}^{-2}$ (0.7–10.0 keV), assuming a photon index of ~ 1 .

5.1.26. *XTE J0052–725 and the other 46.4-s pulsar*

Corbet et al. (2002) reported the discovery of two new transient pulsars with periods of 82.4(2) s and 46.4(1) s from RXTE observations. Their transient nature and the intensity of ~ 1.5 mCrab indicate that these are probably XBPs. The position of the 82.4-s pulsar, XTE J0052–725, was determined with an error box of $\sim 2' \times 8'$. We found no ASCA source in the error box. The position of the 46.4-s pulsar, for which no name was given, was not well determined (Corbet et al. 2002).

5.1.27. *XTE SMC95*

Laycock et al. (2002) carried out monitoring observations of the SMC with RXTE, and discovered a new X-ray pulsar (XTE SMC95) with a period of 95 s. The spectrum was found to be hard with $\Gamma \sim 1.5$. Multiple observations on the same position revealed its transient nature. All of the information indicates that XTE SMC95 is an XBP (probably a Be-XBP because of the transient nature). Because the uncertainty of the position is very large ($\sim 2^\circ \times 0^\circ.2$), the source location should be determined by future studies.

5.1.28. *RX J0117.6–7330*

RX J0117.6–7330 was serendipitously discovered in a ROSAT PSPC observation (Clark et al. 1996). The luminosity was $2.3 \times 10^{37} \text{erg s}^{-1}$ between 0.2–2.5 keV at that time (Clark et al. 1997), and was found to diminish by a factor of over 100 within one year. Macomb et al. (1999) discovered coherent pulsations with a ~ 22.07 s period from the same data, with the aid of the archival data obtained by BASTE onboard CGRO in the same epoch. Strong Balmer emission lines and infrared excess were detected from the companion star in the error circle (Coe et al. 1998), indicating that RX J0117.6–7330 is a Be-XBP. Although the position of RX J0117.6–7330 was covered in ASCA observations A and C, no X-ray emissions were detected. It was difficult to estimate the upper limits of the flux because of the contamination from SMC X-1, which is located only $\sim 5'$ away from RX J0117.6–7330.

5.2. *SNRs*

We give brief comments on the eight SNRs detected with ASCA. Since no new information is obtained for 0056–725 and 0102–723, we merely give the same comments as described in Yokogawa et al. (2000e).

5.2.1. *No. 21 — 0045–734 (N19)*

A ROSAT HRI image shows that X-ray emission from 0045–734 is concentrated within the diffuse radio emission (Yokogawa et al. 2002); thus, this SNR would be classified as a “cen-

trally brightened” SNR defined by Williams et al. (1999). Yokogawa et al. (2002) analyzed the SIS spectrum with NEI (non-equilibrium ionization) plasma models, and found overabundances of some elements which are consistent with the nucleosynthesis of a type-II SN. In spite of the overabundance, the plasma age was found to be large, $\gtrsim 3 \times 10^4$ yr. An evolutionary scenario for such old and overabundant SNRs is proposed by Yokogawa et al. (2002).

5.2.2. No. 23 — 0046–735

Both a power-law model and a thermal CIE model could describe the GIS spectrum well due to highly limited statistics. However, we adopted a thermal model because the derived temperature is reasonable for an SNR; the thermal nature of this SNR is thus suggested.

5.2.3. No. 25 — 0047–735

Source and background regions for 0047–735 were carefully chosen to avoid contamination from the nearby pulsar AX J0049–732. As a result, the extracted SIS spectrum had rather poor statistics, which probably caused a non-detection of emission lines (subsubsection 4.2.3). Thus, we also used the GIS spectra (in obs. F and Q) to compensate for the poor statistics of the SIS spectrum, and carried out a simultaneous fitting.

The spectra were well fitted to both the power-law and the CIE thermal model. However, we adopt the thermal model because the best-fit temperature is reasonable for an SNR. This fact indicates that X-ray emission from this SNR has a thermal origin.

5.2.4. No. 36 — 0049–736

In our earlier study (Yokogawa et al. 2000e), this SNR was regarded as a thermal SNR because of its soft spectrum, although no emission lines were detected due to highly limited statistics. Data from new observations (L and Q) allowed us to detect emission lines (subsubsection 4.2.3), and thus the thermal nature is now established. The GIS spectra were well fitted to a CIE thermal model. The bump-like residuals are found at ~ 1.9 keV, which corresponds to the energy of the emission line from He-like Si. However, allowing the Si abundance to be free did not improve the result within the statistical error.

5.2.5. No. 64 — 0056–725

Since fitting the spectrum with a thin thermal plasma model yielded an unusually high temperature of ~ 20 keV, we adopted a power-law model. There is a possibility that X-rays from 0056–725 actually have a non-thermal origin.

5.2.6. No. 66 — 0057–7226 (N66)

Using a ROSAT HRI image, Yokogawa et al. (2002) found that X-ray emission from 0057–7226 is concentrated within the radio shell. The SIS spectrum was well fitted with an NEI plasma model, showing an overabundance of no element (Yokogawa et al. 2002). The plasma age was found to be relatively old, $\gtrsim 6 \times 10^3$ yr.

5.2.7. No. 81 — 0102–723

A detailed analysis of the SIS spectrum of SNR 0102–723 was carried out by Hayashi et al. (1994). Strong emission lines from various elements were detected, which is consistent with this SNR being young. We adopted the same model and determined its flux and luminosity (table 6).

5.2.8. No. 82 — 0103–726

A ROSAT HRI image shows that X-rays from 0103–726 exhibit faint emission along the radio shell, in addition to more prominent emission concentrated at the center of the shell (Yokogawa et al. 2002). The SIS spectrum was well fitted with NEI plasma models. As for 0045–734 (subsubsection 5.2.1), Yokogawa et al. (2002) found that some elements are overabundant, which is consistent with the nucleosynthesis of a type-II SN, and that the plasma age is large, $\gtrsim 1 \times 10^4$ yr.

5.3. Other Interesting Sources

5.3.1. No. 22 — AX J0048.2–7309

AX J0048.2–7309 was detected in two observations (F and Q) and shows a hard spectrum ($\Gamma \sim 1$) and a flux variability with a factor of ~ 5 (table 6). In addition, we found an emission-line object, No. 215 in Meyssonier and Azzopardi (1993), in the error circle of AX J0048.2–7309. All the information suggests that this source is probably a Be-XBP. Follow-up observations for pulsation searches and optical identification are thus encouraged.

Although the GIS spectra were well fitted to a simple power-law, there remains a bump-like residual in the vicinity of 6–7 keV. In order to examine the existence of an emission line, we used only the data of obs. Q, which has much better statistics. We added a narrow Gaussian and fitted the spectrum, and then determined the center energy and the equivalent width of the Gaussian to be 6.6 (6.4–6.9) keV and 240 (40–440) eV, respectively. However, the significance of the Gaussian is only $\sim 90\%$ in the F -test, thus the existence of the emission line is still not clear. A confirmation of the existence of the emission line would further strengthen the X-ray binary nature of this source.

5.3.2. No. 105 — AX J0128.4–7329

AX J0128.4–7329 is located near the center of an expanding supergiant shell, SMC-1, which has a diameter of $\sim 1^\circ$ (Meaburn 1980). Wang and Wu (1992) reported that the X-ray emission from AX J0128.4–7329 appears to be diffuse in an Einstein IPC image, and that the spectral hardness ratio indicates a temperature of ~ 0.8 keV if the absorption column density is assumed to be 3×10^{20} cm $^{-2}$.

Since the GIS spectrum has rather limited statistics, no rigid constraint was obtained for the spectral parameters. When we fitted the spectrum with a CIE thermal model, a temperature of 2.6 (0.9–10) keV was obtained, which is marginally consistent with the argument of Wang

and Wu (1992). Since half of the GIS FOV is polluted by stray light, which is probably from SMC X-1, it is difficult to know the extent of AX J0128.4–7329.

6. Discussion

6.1. Period Distribution of XBPs

We have shown that at least 26 out of the 30 X-ray pulsars in the SMC are XBPs, probably with a high-mass star companion. Recently, Liu et al. (2000) compiled a catalogue of Galactic HMXBs in which 49 XBPs are included (in this paper we do not regard 4U 2206+543 as an XBP because of the non detection of pulsations in a further study by Corbet & Peele, 2001). In addition, we investigated the recent literatures and found four new XBPs, AX J1740.1–2847, XTE J1543–568, SAX J2239.3+6116, and AX J1841.0–0536 (Sakano et al. 2000; Finger, Wilson 2000; In ’t Zand et al. 2001; Bamba et al. 2001). In figure 9 we show the distribution of pulse periods of the 53 XBPs in the Galaxy and 26 in the SMC. The average periods are ~ 430 s and ~ 130 s for XBPs in the Galaxy and in the SMC, respectively. The significant difference is mainly caused by the lack of long period pulsars ($\gtrsim 1000$ s) in the SMC.

We investigated the literature and found that Galactic XBPs with periods longer than 755 s (the longest period in the SMC) are all faint (table 7). Their luminosities, $\lesssim 10^{35}$ erg s $^{-1}$, correspond to $\lesssim 3 \times 10^{-13}$ erg s $^{-1}$ cm $^{-2}$ at the SMC distance, which are below, or only slightly above, the detection limit of this study. Therefore, we suggest that the lack of long-period pulsars in the SMC are merely due to the selection effect. This suggestion is supported by the fact that long-period pulsars in the SMC are also relatively faint (see subsections 5.1.5 and 5.1.18).

6.2. Source Classification

6.2.1. Criteria for source classification

We classify the 106 ASCA sources into several source classes, which are given in the “Class” column in table 5. Definitions of the classes are the following.

XBPs (“BP” in table 5) are the 18 pulsars having a long pulse period (~ 1 –1000 s), hard spectrum ($\Gamma \sim 1$), flux variability, and/or an optical counterpart, as described in subsection 5.1. No. 72 (CXOU J0110043.1–721134) is proposed to be an AXP (Lamb et al. 2002b); we thus designate this source as “AXP”. Pulsars which are not definitely regarded as XBPs or AXPs are designated as “P”. Thermal SNRs (“TS”) are the five SNRs from which emission lines of ionized atoms were detected in subsection 4.2.3. The other SNRs with no significant emission line are classified as radio SNRs (“RS”). Candidates for XBPs and thermal SNRs (“BPc” and “TSc”) are defined in subsection 6.2.3.

Nonpulsating HMXBs (“NH”) and candidates (“NHc”) are defined by the optical counterparts and flux variability as summarized in table 8. Grades from A to E are assigned

according to the following criteria. Grade A and B sources are X-ray sources with a Be or a supergiant star companion. Flux variability has been known for grade A’s, while not for grade B’s. Grade C and D sources consist of X-ray sources having an emission-line object (Be star candidate) as a counterpart, which are catalogued in Haberl and Sasaki (2000). Again, flux variability has been known for grade C’s while not for grade D’s. Grade E sources also have an emission-line object counterpart, but other possibilities (AGN or active corona of a late type star) are proposed by Haberl and Sasaki (2000). In table 5, we designate grade A and B sources as “NH” and grade C and D sources as “NHc”.

Foreground stars (“FS”) and AGN (“AGN”) are defined merely based on positional coincidence of ROSAT sources of these classes (Sasaki et al. 2000 and references therein). Sources which do not fall into any classes are designated as “UN” (unclassified sources); UN(m) and UN(h) are defined in subsection 6.2.3.

6.2.2. Classification by hardness ratio

In our earlier paper (Yokogawa et al. 2000e), we found a relation between source classes and their spectral hardness ratio (HR): XBPs and thermal SNRs fall in the regions of $0.2 \lesssim \text{HR} \lesssim 0.6$ (“XBP region”) and $-1.0 \lesssim \text{HR} \lesssim -0.6$ (“thermal SNR region”), respectively, while Crab-like SNRs and BH binaries stay between these regions ($\text{HR} \sim 0$). Having the increased number of sources, we investigated whether the same relation still holds. Figure 10 shows a plot of HR against the observed luminosity L_{obs} , defined as $L_{\text{obs}} = F_x \times 4\pi d^2$, where d is the distance to the SMC (60 kpc). We find that seven XBPs and one thermal SNR that were newly added from the new data also satisfy the same relation. It is worth noting that most of the new XBPs and thermal SNR are relatively faint with $L_{\text{obs}} \lesssim 10^{36}$ erg s⁻¹, and that the classifications of these sources are mainly based on a very long ASCA observation or an XMM-Newton observation, which provides a better S/N ratio. This fact implies that the relation between source classes and HR is still valid for fainter sources.

6.2.3. Candidates for XBPs, thermal SNRs, and background AGN

Using the HR– L_{obs} plot (figure 10), we regard sources in the XBP (or thermal SNR) region as candidates for XBPs (or thermal SNRs). We find 19 XBP candidates and four thermal SNR candidates, which are designated as BPc and TSc in table 5, respectively. No. 91 is excluded from the XBP candidates because of the positional coincidence of an AGN. Although the HRs of No. 2 and No. 13⁴ are -1 , we do not classify them as thermal SNRs because of their large HR errors. No. 25 also has a large HR error ($\text{HR} = -1.00 \pm 1.38$), but we classify this source as a thermal SNR because its SIS spectrum is typical of this class and because it has a radio SNR counterpart (0047–735).

Nonpulsating HMXBs and their candidates (table 8) are all located within or near the

⁴ These sources are not plotted in figure 10 because L_{obs} is not derived (see subsection 4.2.5).

XBP region, thus are very promising targets for pulsation searches. Non-detection of pulsations from these sources is very likely due to the poor statistics. The detection of pulsations from low-flux sources AX J0049.5–7323, AX J0051.6–7311, and RX J0101.3–7211 well demonstrates the necessity of high sensitivity observations (see subsections 5.1.5, 5.1.8, and 5.1.18).

Two radio SNRs (0046–735 and 0047–735) are found among the thermal SNR candidates. The spectra of these sources have very limited statistics, and thus were not classified as thermal SNRs in subsection 4.2.3. Another radio SNR, 0056–725, is located within the XBP region. Therefore, X-rays from this source may be attributed to an unresolved XBP in the radio SNR 0056–725, such as 1SAX J0103.2–7209.

AGN and foreground stars are mostly located between the XBP and thermal SNR regions. Crab-like SNRs and BH binaries are also found at $HR \sim 0$ (Yokogawa et al. 2000e). LMXBs have spectra of $\Gamma \sim 2$, which are similar to those of Crab-like SNRs; thus, LMXBs are also expected to be located at $HR \sim 0$. We find 33 unclassified sources in this medium HR regime ($-0.6 < HR < 0.2$; “UN(m)” in table 5; hereafter medium HR sources). Are they SMC members, or are they background/foreground sources? To address this question, we used the $\log N$ – $\log S$ relation from the ASCA Medium-Sensitivity Survey (Ueda et al. 1999). It is difficult to determine the accurate detection limit for our survey because of various uncertainties, such as contamination from bright sources, and the position-dependent efficiency of the detector. Therefore, we only make a rough estimation from figure 10 that the detection limit is 10^{-13} – 10^{-12} erg s $^{-1}$ cm $^{-2}$ (4×10^{34} – 4×10^{35} erg s $^{-1}$). With this limit, several AGN could be detected in the GIS FOV in each observation; we can thus expect that several tens of AGN could be detected in our SMC survey. Therefore, it is likely that most of the 33 medium HR sources are background AGN. This conclusion is independently supported by the spatial distribution of these sources, as shown in subsection 6.4.

The very hard regime ($HR > 0.6$) contains seven unclassified sources (“UN(h)” in table 5; hereafter, very hard sources). Even if a source has a hard spectrum with $\Gamma = 1.0$, a large absorption column of $N_H > 10^{22}$ cm $^{-2}$ is required for HR to exceed 0.6. Therefore, we regard these seven very hard sources as highly absorbed objects.

6.3. Source Populations in the SMC and in Our Galaxy

6.3.1. Basic data

We have shown that most of the ASCA sources in the SMC region are classified as XBPs (mostly Be-XBPs), nonpulsating HMXBs, and SNRs, in addition to foreground stars and background AGN. In order to make a comparison of source populations in the SMC and in our Galaxy, we combined the results of our study with various catalogues compiled by other authors. The source classes included in this discussion are summarized in table 9: HMXBs (XBPs and nonpulsating HMXBs), LMXBs, and SNRs (Crab-like and others).

HMXBs in the SMC consist of 26 XBPs (subsection 5.1) and eight nonpulsating HMXBs

(grades A and B in table 8). Candidates for HMXBs are a combination of the 19 XBP candidates defined in this study (BPc in table 5) and the grade C and D sources in table 8. Here, we regard the XBPs (and candidates) with an unknown optical counterpart as HMXBs, because most XBPs hitherto found are HMXBs (e.g., Bildsten et al. 1997). Evidence for LMXBs has not been detected from any source in the SMC. SNRs in the SMC have been surveyed by Mathewson et al. (1983, 1984) in the radio band and later by Filipović et al. (1998a) in both the radio and X-ray bands; as a result 14 SNRs have been detected. Five SNR candidates have been found by Filipović et al. (1998b) and Haberl et al. (2000). In addition, two thermal SNR candidates defined in this study (No. 6 and No. 45) have no radio SNR counterpart, and are thus candidates for new SNRs. No evidence for Crab-like SNRs has been found.

HMXBs in our Galaxy are the 53 XBPs described in subsection 6.1 plus ~ 30 nonpulsating HMXBs catalogued in Liu et al. (2000). Most complete LMXB catalogue is Liu et al. (2001), in which ~ 130 LMXBs are contained. Green (2000) has compiled the most complete catalogue of 225 radio SNRs in our Galaxy. Among them, about 10 are associated with a rotation-powered X-ray pulsar, thus are regarded as Crab-like SNRs. In addition, some new SNRs have been discovered in the X-ray band with ROSAT, ASCA, XMM-Newton, and Chandra. We tentatively expect 100 SNR candidates to be discovered in the near future (Aschenbach 1996).

6.3.2. Comparison of the source populations

Based on table 9, we compare the source populations in the SMC and in our Galaxy from various aspects.

Since the mass of the SMC is about 1/100th the mass of our Galaxy (e.g., Westerlund 1997), the source numbers in our Galaxy should be divided by 100 for a simple comparison (as in the second row of table 9). As has been pointed out by several authors (Schmidtke et al. 1999; Yokogawa et al. 2000e), the normalized number of HMXBs is found to be much higher in the SMC. On the other hand, the normalized numbers of LMXBs are comparable in the two galaxies, although the statistics are limited. Considering the detection limit of our survey, we conclude that the significant differences in the source numbers are not attributable to a selection effect (see subsection 5.4 of Yokogawa et al. 2000e for more detail). HMXBs are descendants of massive star binaries with ages of $\sim 10^7$ yr, while LMXBs comprise a much older population probably with ages of $\gtrsim 10^9$ yr. Therefore, we propose that the star forming rate was comparable between the two galaxies in a very old epoch ($\gtrsim 10^9$ yr ago), and then more recently ($\sim 10^7$ yr ago) it was much higher in the SMC.

HMXBs and type-II SNRs are both descendants of young massive stars, but the duration of being X-ray emitters would be highly different ($\sim 10^6$ – 10^7 yr for the former while $\sim 10^5$ yr for the latter). Therefore, the number ratio between HMXBs and type-II SNRs probably indicates a change of the star formation rate in a very recent epoch ($\lesssim 10^7$ yr ago). We assume that SNRs in the SMC are all type-II because of the spatial distribution discussed in subsection 6.4,

thus the number ratio of [HMXBs]/[type-II SNRs] (hereafter, H/II) in the SMC is $\approx 2-3$. As for our Galaxy, H/II is estimated to be $\approx 0.5-0.7$, if we simply assume that 50% of Galactic SNRs are type-II. This assumption is reasonable because many SNRs are concentrated in the Galactic plane (e.g., $\sim 60\%$ are at $|b| < 1^\circ$; Green 2000), and are thus considered to be mainly type-II. The much larger value of H/II in the SMC implies that there was a dramatic decline of the star-forming rate in a very recent epoch ($\lesssim 10^7$ yr ago), following active star formation of $\sim 10^7$ yr ago described above.

Although both HMXBs and Crab-like SNRs are direct descendants of massive stars, the number ratios of these classes are significantly different: 10/83 in our Galaxy and 0/34 in the SMC (0/74 when the HMXB candidates are included). If the ratio is identical between galaxies, at least several Crab-like SNRs should be found in the SMC. Crab-like SNRs in the SMC, if exist, would be found in the medium HR regime ($HR \sim 0$), where those in the LMC are located (Yokogawa et al. 2000e). Therefore, some of the 33 medium HR sources may be Crab-like SNRs; non-detection of pulsations could be due to limited statistics. High-sensitivity observations of those sources with a good time resolution would thus be fruitful. In addition, high-resolution radio surveys to search for plerionic emission are also encouraged. If, on the other hand, Crab-like SNRs are really lacking in the SMC, it may imply that the binary frequency of massive stars is much higher in the SMC because Crab-like SNRs and HMXBs are descendants of single and binary massive stars, respectively. A higher binary frequency can in part be a cause of the higher number ratio of HMXBs to type-II SNRs mentioned above.

6.4. *Spatial Distribution of Various Classes of Sources*

We investigated the spatial distributions of four classes of sources: HMXBs, SNRs, AGN plus medium HR sources, and very hard sources. In this subsection, ‘‘HMXBs’’ include the XBP, nonpulsating HMXBs, and HMXB candidates in table 9, while ‘‘SNRs’’ include the Crab-like and other SNRs and SNR candidates in table 9. Medium HR sources and very hard sources are defined in subsection 6.2.3.

We show the spatial distribution of HMXBs in figure 11a. We find that most HMXBs are concentrated in the optical main body, and $\sim 10\%$ are located in the eastern wing. Maragoudaki et al. (2001) carried out an optical survey of the SMC and derived spatial distributions of stars in seven ranges of ages from $> 2 \times 10^9$ yr to $< 8 \times 10^6$ yr. They found that very old stars have a smooth and spheroidal distribution, while younger stars are concentrated in the main body and the eastern wing. Comparing figure 11a with their results, we find that the distribution of the HMXBs well resembles that of younger stars, especially stars with ages of $(1.2-3) \times 10^7$ yr (figure 12). This is naturally expected because HMXBs are descendants of massive (young) stars.

The spatial distribution of SNRs shown in figure 11b is very similar to that of HMXBs. Therefore, we regard that most of the SNRs are descendants of massive stars (i.e., type-II

SNRs). This is consistent with the fact that so far type-Ia SNRs have not been found in the SMC, while three SNRs have type-II origin (subsection 5.2).

We also investigated the distribution of the 33 medium HR sources and five AGN as shown in figure 11c. The distribution is relatively uniform, which exhibits a clear contrast with HMXBs and SNRs and is qualitatively consistent with the distribution of old stars ($> 2 \times 10^9$ yr) found by Maragoudaki et al. (2001). This fact implies either that (1) most of the medium HR sources are unrelated to the SMC, i.e., background or foreground sources, or that (2) they represent a population much older than the HMXBs. Scenario (1) is consistent with the estimate from the $\log N$ – $\log S$ relation discussed in subsection 6.2.3. However, taking account of the large uncertainty in the above estimate, there still remains a possibility that some of the medium HR sources represent an older population, probably LMXBs. Since the number of LMXBs has a relatively large impact on the star-forming activity in the old epoch (see subsection 6.3.2), follow-up observations of these medium HR sources are encouraged.

The distribution of the seven very hard sources shown in figure 11d seems to be as uniform as that of the AGN and the medium HR sources, although the number of sources is highly limited. Therefore, the very hard sources may be unrelated to the SMC, i.e., background or foreground sources. Considering the suggestion that these sources should be highly absorbed (see 6.2.3), we propose that most of them are Seyfert 2 galaxies. We thus encourage optical follow-up observations of these sources.

J.Y., K.I., and M.T. were financially supported by JSPS Research Fellowship for Young Scientists. We are grateful to Prof. Fukazawa for his help when revising the manuscript. We retrieved ROSAT data from the HEASARC Online System which is provided by NASA/GSFC.

References

- Aschenbach, B. 1996, MPE Report, 263, 213
- Bamba, A., Yokogawa, J., Ueno, M., Koyama, K., & Yamauchi, S. 2001, PASJ, 53, 1179
- Bildsten, L., Balser, D. S., Chiu, J., Finger, M. H., Koh, D. T., Nelson, R. W., Prince, T. A., Rubin, B. C., et al. 1997, ApJS, 113, 367
- Buckley, D. A. H., Coe, M. J., Stevens, J. B., van der Heyden, K., Angelini, L., White, N., & Giommi, P. 2001, MNRAS, 320, 281
- Burke, B. E., Mountain, R. W., Daniels, P. J., Cooper, M. J., & Dolat, V. S. 1994, IEEE Trans. Nucl. Sci., 41, 375
- Chakrabarty, D., Levine, A. M., Clark, G. W. & Takeshima, T. 1998a, IAU Circ., 7048
- Chakrabarty, D., Takeshima, T., Ozaki, M., Paul, B., & Yokogawa, J. 1998b, IAU Circ., 7062
- Clark, G., Doxsey, R., Li, F., Jernigan, J. G., & van Paradijs, J. 1978, ApJ, 221, L37
- Clark, G., Remillard, R., & Woo, J. 1996, IAU Circ., 6282
- Clark, G. W., Remillard, R. A., & Woo, J. W. 1997, ApJ, 474, L111
- Coe, M. J., Buckley, D. A. H., Charles, P. A., Southwell, K. A., & Stevens, J. B. 1998, MNRAS, 293,

- Coe, M. J., Haigh, N. J., & Reig, P. 2000, *MNRAS*, 314, 290
- Coe, M. J., Haigh, N. J., Laycock, S. G. T., Negueruela, I., & Kaiser, C. R. 2002, *MNRAS*, 332, 473
- Coe, M. J., & Orosz, J. A. 2000, *MNRAS*, 311, 169
- Corbet, R. H. D. 1984, *A&A*, 141, 91
- Corbet, R., Markwardt, C. B., Marshall, F. E., Laycock, S., & Coe, M. 2002, *IAU Circ.*, 7932
- Corbet, R. H. D., Marshall, F. E., Coe, M. J., Laycock, S., & Handler, G. 2001b, *ApJ*, 548, L41
- Corbet, R., Marshall, F. E., Lochner, J. C., Ozaki, M., & Ueda, Y. 1998, *IAU Circ.*, 6803
- Corbet, R., Marshall, F. E., & Markwardt, C. B. 2001a, *IAU Circ.*, 7562
- Corbet, R. H. D., & Peele, A. G. 2001, *ApJ*, 562, 936
- Cowley, A. P., Schmidtke, P. C., McGrath, T. K., Ponder, A. L., Fertig, M. R., Hutchings, J. B., & Crampton, D. 1997, *PASP*, 109, 21
- Crampton, D., Hutchings, J. B., & Cowley, A. P. 1978, *ApJ*, 223, L79
- Cusumano, G., Maccarone, M. C., Nicastro, L., Sacco, B., & Kaaret, P. 2000, *ApJ*, 528, L25
- Davies, R. D., Elliott, K. H., & Meaburn, J. 1976, *MmRAS*, 81, 89
- Dotani, T., Yamashita, A., Ezuka, H., Takahashi, K., Crew, G., Mukai, K., & the SIS Team 1997, *ASCA News*, 5, 14
- Filipović, M. D., Haynes, R. F., White, G. L., & Jones, P. A. 1998b, *A&AS*, 130, 421
- Filipović, M. D., Pietsch, W., Haynes, R. F., White, G. L., Jones, P. A., Wielebinski, R., Klein, U., Dennerl, K., Kahabka, P., & Lazendić, J. S. 1998a, *A&AS*, 127, 119
- Filipović, M. D., Pietsch, W., & Haberl, F. 2000a, *A&A*, 361, 823
- Filipović, M. D., Haberl, F., Pietsch, W., & Morgan, D. H. 2000b, *A&A*, 353, 129
- Finger, M. H., & Wilson, C. A. 2000, *IAU Circ.*, 7366
- Gotthelf, E. V., Ueda, Y., Fujimoto, R., Kii, T., & Yamaoka, K. 2000, *ApJ*, 543, 417
- ‘A Catalogue of Galactic Supernova Remnants (2000 August version)’, Mullard Radio Astronomy Observatory, Cavendish Laboratory, Cambridge, United Kingdom (available on the World-Wide-Web at <http://www.mrao.cam.ac.uk/surveys/snrs/>)
- Haberl, F., Angelini, L., Motch, C., & White, N. E. 1998, *A&A*, 330, 189
- Haberl, F., Filipovic, M. D., Pietsch, W., & Kahabka P. 2000, *A&AS*, 142, 41
- Haberl, F., & Sasaki, M. 2000, *A&A*, 359, 573
- Hayashi, I., Koyama, K., Ozaki, M., Miyata, E., Tsunemi, H., Hughes, J. P., & Petre, R. 1994, *PASJ*, 46, L121
- Henize, K. G. 1956, *ApJS*, 2, 315
- Hirayama, M., Nagase, F., Gunji, S., Sekimoto, Y., Saito, Y. 1996, *ASCA News*, 4, 18
- Hughes, J. P. 1994, *ApJ*, 427, L25
- Hughes, J. P., & Smith, R. C. 1994, *AJ*, 107, 1363
- Imanishi, K., Yokogawa, J., & Koyama, K. 1998, *IAU Circ.*, 7040
- Imanishi, K., Yokogawa, J., Tsujimoto, M., & Koyama, K. 1999, *PASJ*, 51, L15
- Inoue, H., Koyama, K., & Tanaka, Y. 1983, in *IAU Symposium 101, Supernova Remnants and their X-Ray Emission*, ed. J. Danziger & P. Gorenstein (Dordrecht: D. Reidel Publishing Co.), 535

- In 't Zand, J. J. M., Halpern, J., Eracleous, M., McCollough, M., Augusteign, T., Remillard, R. A., Heise, J. 2000, *A&A*, 361, 85
- In 't Zand, J. J. M., Swank, J., Corbet, R. H. D., & Markwardt, C. B. 2001, *A&A*, 380, L26
- Israel, G. L., Campana, S., Covino, S., Dal Fiume, D., Gaetz, T. J., Mereghetti, S., Oosterbroek, T., Orlandini, M., et al. 2000, *ApJ*, 531, L131
- Israel, G. L., Campana, S., Cusumano, G., Frontera, F., Orlandini, M., Santangelo, A., & Stella, L. 1998b, *A&A*, 334, L65
- Israel, G. L., Stella, L., Angelini, L., White, N. E., Giommi, P., & Covino, S. 1997, *ApJ*, 484, L141
- Israel, G. L., Stella, L., Campana, S., Covino, S., Ricci, D., & Oosterbroek, T. 1998a, *IAU Circ.*, 6999
- Israel, G. L., Stella, L., Covino, S., Campana, S., & Mereghetti, S. 1999, *IAU Circ.*, 7101
- Kaaret, P., Piraino, S., Halpern, J., & Eracleous, M. 1999, *ApJ*, 523, 197
- Kahabka, P. 2000, *A&A*, 354, 999
- Kahabka, P., & Pietsch, W. 1996, *A&A*, 312, 919
- Kahabka, P., & Pietsch, W. 1998, *IAU Circ.*, 6840
- Kohn, M., Yokogawa, J., & Koyama, K. 2000, *PASJ*, 52, 299
- Lamb, R. C., Fox, D. W., Macomb, D. J., & Prince, T. A. 2002b, *ApJ*, 574, L29
- Lamb, R. C., Prince, T. A., Macomb, D. J. & Finger, M. H. 1999, *IAU Circ.*, 7081
- Lamb, R. C., Macomb, D. J., Prince, T. A., & Majid, W. A. 2002a, *ApJ*, 567, L129
- Laycock, S., Corbet, R. H. D., Perrodin, D., Coe, M. J., Marshall, F. E., & Markwardt, C. 2002, *A&A*, 385, 464
- Liu, Q. Z., van Paradijs, J., & van den Heuvel, E. P. J. 2000, *A&AS*, 147, 25
- Liu, Q. Z., van Paradijs, J., & van den Heuvel, E. P. J. 2001, *A&A*, 368, 1021
- Lochner, J. C. 1998, *IAU Circ.*, 6858
- Lochner, J. C., Marshall, F. E., Whitlock, L. A., & Brandt, N. 1998, *IAU Circ.*, 6814
- Lucke, R., Yentis, D., Friedman, H., Fritz, G., & Shulman, S. 1976, *ApJ*, 206, L25
- Macomb, D. J., Finger, M. H., Harmon, B. A., Lamb, R. C., & Prince, T. A. 1999, *ApJ*, 518, L99
- Maragoudaki, F., Kontizas, M., Morgan, D. H., Kontizas, E., Dapergolas, A., & Livanou, E. 2001, *A&A*, 379, 864
- Marshall, F. E., Boldt, E. A., Holt, S. S., Mushotzky, R. F., Pravdo, S. H., Rothschild, R. E., & Serlemitsos, P. J. 1979, *ApJS*, 40, 657
- Marshall, F. E., & Lochner, J. C. 1998, *IAU Circ.*, 6818
- Marshall, F. E., Lochner, J. C., & Takeshima, T. 1997, *IAU Circ.*, 6777
- Mathewson, D. S., Ford, V. L., Dopita, M. A., Tuohy, I. R., Long, K. S., & Helfand, D. J. 1983, *ApJS*, 51, 345
- Mathewson, D. S., Ford, V. L., Dopita, M. A., Tuohy, I. R., Mills, B. Y., & Turtle, A. J. 1984, *ApJS*, 55, 189
- Meaburn, J. 1980, *MNRAS*, 192, 365
- Mereghetti, S., Tiengo, A., Israel, G. L., & Stella, L. 2000, *A&A*, 354, 567
- Meyssonier, N., & Azzopardi, M. 1993, *A&AS*, 102, 451
- Mitsuda, K., Inoue, H., Koyama, K., Makishima, K., Matsuoka, M., Ogawara, Y., Shibasaki, N., Suzuki, K., Tanaka, Y., & Hirano, T. 1984, *PASJ*, 36, 741

Motch, C., Haberl, F., Dennerl, K., Pakull, M., & Janot-Pacheco, E. 1997, *A&A*, 323, 853
 Murdin, P., Morton, D. C., & Thomas, R. M. 1979, *MNRAS*, 1979, 186
 Murphy, M. T., & Bessell, M. S. 2000, *MNRAS*, 311, 741
 Nagase, F. 1989, *PASJ*, 41, 1
 Ohashi, T., Ebisawa, K., Fukazawa, Y., Hiyoshi, K., Horii, M., Ikebe, Y., Ikeda, H., Inoue, H., et al. 1996, *PASJ* 48, 157
 Ozaki, M., Corbet, R. H. D., Marshall, F. E., & Lochner, J. C. 2000, *Adv. Space Res.*, 25, No. 3/4, 425
 Paul, B., Nagase, F., Endo, T., Dotani, T., Yokogawa, J., & Nishiuchi, M. 2002, *ApJ*, 579, 411
 Petro, L., Feldman, F., & Hiltner, W. A. 1973, *ApJ*, 184, L123
 Raymond, J. C., & Smith, B. W. 1977, *ApJS*, 35, 419
 Reig, P., Chakrabarty, D., Coe, M. J., Fabregat, J., Negueruela, I., Prince, T. A., Roche, P., & Steele, I. A. 1996, *A&A*, 311, 879
 Reig, P., & Roche, P. 1999, *MNRAS*, 306, 100
 Russell, S. C., & Dopita, M. A. 1992, *ApJ*, 384, 508
 Sakano, M. 2000, Ph.D. Thesis, Kyoto University
 Sakano, M., Torii, K., Koyama, K., Maeda, Y., & Yamauchi, S. 2000, *PASJ*, 52, 1141
 Santangelo, A., Cusumano, G., Dal Fiume, D., Israel, G. L., Stella, L., Orlandini, M., & Parmar, A. N. 1998, *A&A*, 338, L59
 Sasaki, M., Haberl, F., Keller, S., & Pietsch, W. 2001, *A&A*, 369, L29
 Sasaki, M., Haberl, F., & Pietsch, W. 2000, *A&AS*, 147, 75
 Schmidtke, P. C., Cowley, A. P., Crane, J. D., Taylor, V. A., McGrath, T. K., Huchings, J. D., & Crampton, D. 1999, *AJ*, 117, 927
 Serlemitsos, P. J., Jalota, L., Soong, Y., Kunieda, H., Tawara, Y., Tsusaka, Y., Suzuki, H., Sakima, Y., et al. 1995, *PASJ*, 47, 105
 Southwell, K. A., & Charles, P. A. 1996, *MNRAS*, 281, L63
 Stevens, J. B., Coe, M. J., & Buckley, D. A. H. 1999, *MNRAS*, 309, 421
 Tanaka, Y., Inoue, H., & Holt, S. S. 1994, *PASJ* 46, L37
 Telting, J. H., Waters, L. B. F. M., Roche, P., Boogert, A. C. A., Clark, J. S., de Martino, D., & Persi, P. 1998, *MNRAS*, 296, 785
 Torii, K., Kohmura, T., Yokogawa, J., & Koyama, K. 2000b, *IAU Circ.*, 7441
 Torii, K., Yokogawa, J., Imanishi, K., & Koyama, K. 2000a, *IAU Circ.*, 7428
 Tsujimoto, M., Imanishi, K., Yokogawa, J., Koyama, K. 1999, *PASJ*, 51, L21
 Tucholke H.-J., de Boer K. S., & Seitter W. C. 1996, *A&AS*, 119, 91
 Ueda, Y., Takahashi, T., Inoue, H., Tsuru, T., Sakano, M., Ishisaki, Y., Ogasaka, Y., Makishima, K., et al. 1999, *ApJ*, 518, 656
 Ueno, M., Yokogawa, J., Imanishi, K., & Koyama, K. 2000a, *PASJ*, 52, L63
 Ueno, M., Yokogawa, J., Imanishi, K., & Koyama, K. 2000b, *IAU Circ.*, 7442
 van den Bergh, S. 2000, *PASP*, 112, 529
 Vrtilik, S. D., Raymond, J. C., Boroson, B., Kallman, T., Quaintrell, H., & McCray, R. 2001, *ApJL*, 563, L139

- Wang, Q., & Wu, X. 1992, ApJS, 78, 391
- Westerlund, B. E. 1997, in *The Magellanic Clouds*, (New York: Cambridge University Press), 19
- White, N. E., Swank, J. H., & Holt, S. S. 1983, ApJ, 270, 711
- Whitlock, L., & Lochner, J. C. 1994, ApJ, 437, 841
- Williams, R. M., Chu, Y-H., Dickel, J. R., Petre, R., Smith, R. C., & Tavaréz, M. 1999, ApJS, 123, 467
- Wilson, C. A., & Finger, M. H. 1998, IAU Circ., 7048
- Wojdowski, P., Clark, G. W., Levine, A. M., Woo, J. W., & Zhang, S. N. 1998, ApJ, 502, 253
- Ye, T., Amy, S. W., Wang, Q. D., Ball, L., & Dickel, J. 1995, MNRAS, 275, 1218
- Yokogawa, J. 2002, Ph.D. thesis, Kyoto University, available at <http://www-cr.scphys.kyoto-u.ac.jp/member/jun/job/phd/>
- Yokogawa, J., Imanishi, K., Koyama, K., Nishiuchi, M., & Mizuno, N. 2002, PASJ, 54, 53
- Yokogawa, J., Imanishi, K., Tsujimoto, M., Kohno, M., & Koyama, K. 1999, PASJ, 51, 547
- Yokogawa, J., Imanishi, K., Tsujimoto, M., Nishiuchi, M., Koyama, K., Nagase, F., & Corbet, R. H. D. 2000e, ApJS, 128, 491
- Yokogawa, J., Imanishi, K., Ueno, M., & Koyama, K. 2000a, PASJ, 52, L73
- Yokogawa, J., Paul, B., Ozaki, M., Nagase, F., Chakrabarty, D., & Takeshima, T. 2000d, ApJ, 539, 191
- Yokogawa, J., Torii, K., Imanishi, K., & Koyama, K. 2000b, PASJ, 52, L37
- Yokogawa, J., Torii, K., Kohmura, T., Imanishi, K., & Koyama, K. 2000c, PASJ, 52, L53
- Yokogawa, J., Torii, K., Kohmura, T., & Koyama, K. 2001a, PASJ, 53, L9
- Yokogawa, J., Torii, K., Kohmura, T., & Koyama, K. 2001b, PASJ, 53, 227
- Yokogawa, J., & Koyama, K. 1998a, IAU Circ., 6853
- Yokogawa, J., & Koyama, K. 1998b, IAU Circ., 7028
- Yokogawa, J., & Koyama, K. 1998c, IAU Circ., 7009
- Yokogawa, J., & Koyama, K. 2000, IAU Circ., 7361
- Yoshii, Y., Tsujimoto, T., & Nomoto, K. 1996, ApJ, 462, 266

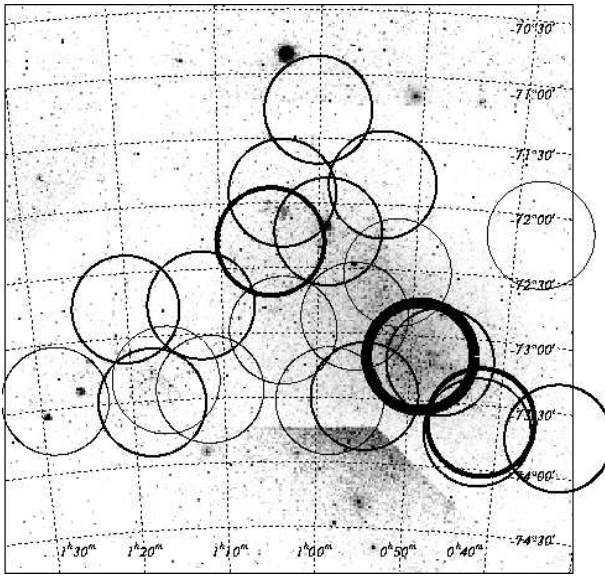


Fig. 1. All observation fields with ASCA GIS superimposed on the optical image of the SMC region from the Digitized Sky Survey (DSS). Equatorial coordinates with an equinox of 2000 are also shown. Each observation field is represented by a 50'-diameter circle, the thickness of which is proportional to the exposure time. The discontinuity seen in the DSS image is an artifact.

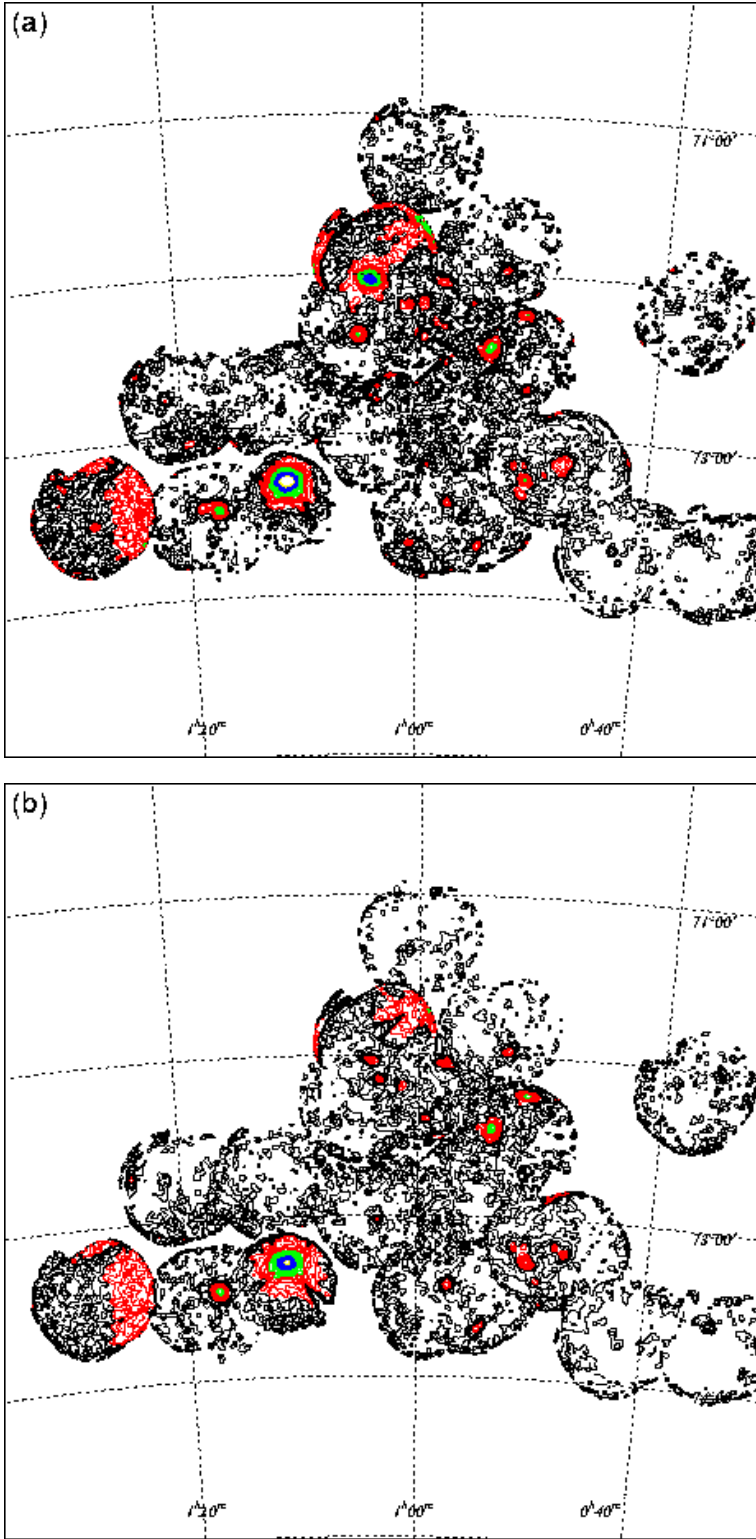


Fig. 2. Mosaic images of the SMC obtained with ASCA GIS in the soft (a: 0.7–2.0 keV) and hard (b: 2.0–7.0 keV) bands, overlaid with equatorial coordinates (J2000). The effects of non-X-ray background, telescope vignetting, and difference of exposure time between observations were corrected. Contour levels are linearly spaced. Of the two observations centered on SMC X-1 (observations A and C), only observation C was used, in which SMC X-1 was much fainter.

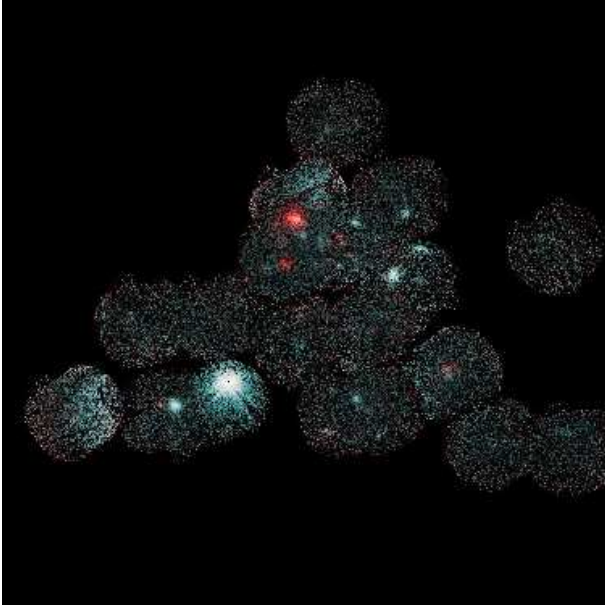


Fig. 3. Two-color X-ray mosaic image of the SMC. Red and blue indicate X-ray photons in the soft (0.7–2.0 keV) and hard (2.0–7.0 keV) bands, respectively.

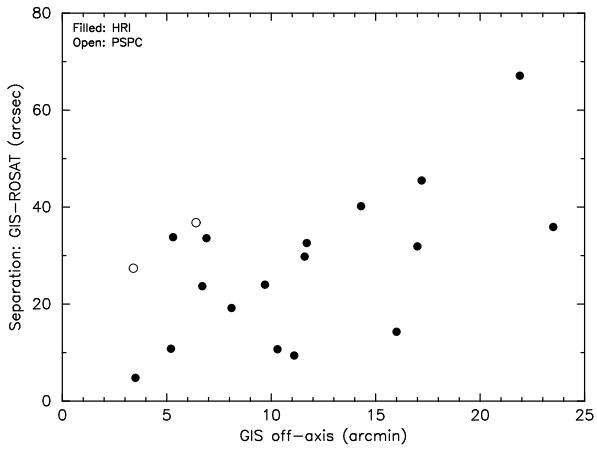


Fig. 4. Plot of the separation angles between the ROSAT–ASCA counterparts as a function of the off-axis angle of the ASCA sources (see table 2). The filled and open circles indicate the sources detected with ROSAT HRI and PSPC, respectively.

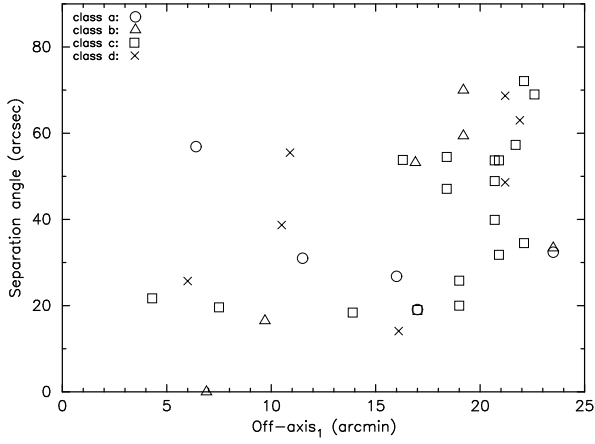


Fig. 5. Plot of the separation angles as a function of the larger off-axis angle (off-axis₁ in table 3) of ASCA sources detected multiple times.

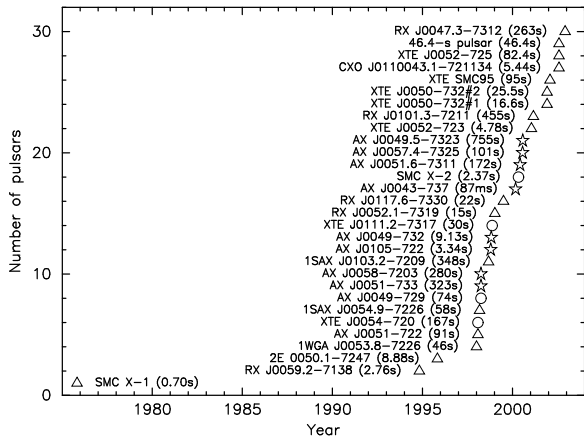


Fig. 6. History of discoveries of X-ray pulsars in the SMC as of 2002 November. The symbols represent the pulsars discovered in this study (stars), the pulsars for which only the positions were determined in this study (circles), and the remainder (triangles).

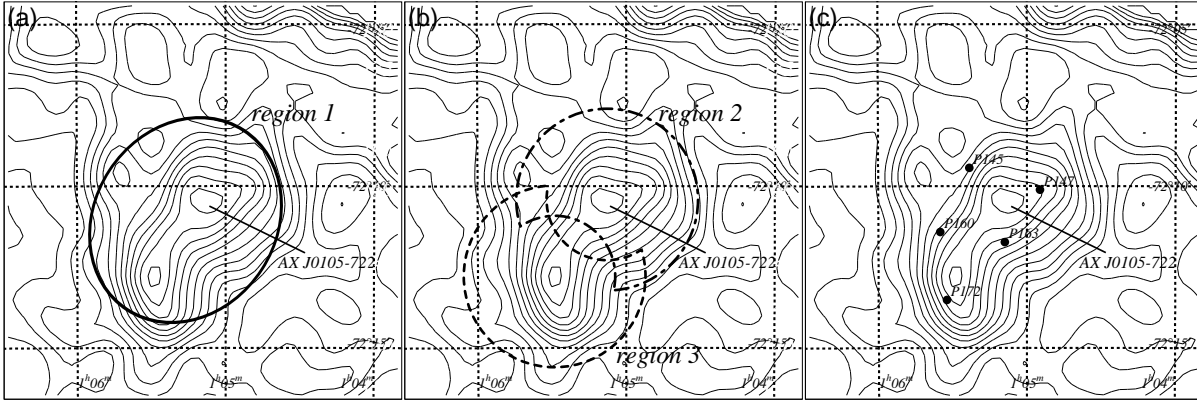


Fig. 7. ASCA GIS contour images around AX J0105–722 in 0.7–7.0 keV, overlaid with the equatorial coordinates (J2000). Two ASCA sources are detected in this image, one of which is AX J0105–722 and the other is No. 84, located at $\sim 3'$ southeast. Regions 1–3 from which event lists were extracted for pulsation searches (see text) are indicated by the ellipse and circles in (a) and (b). The five dots marked with “Pn” in (c) are the ROSAT PSPC sources in Haberl et al. (2000) with an ID number of n .

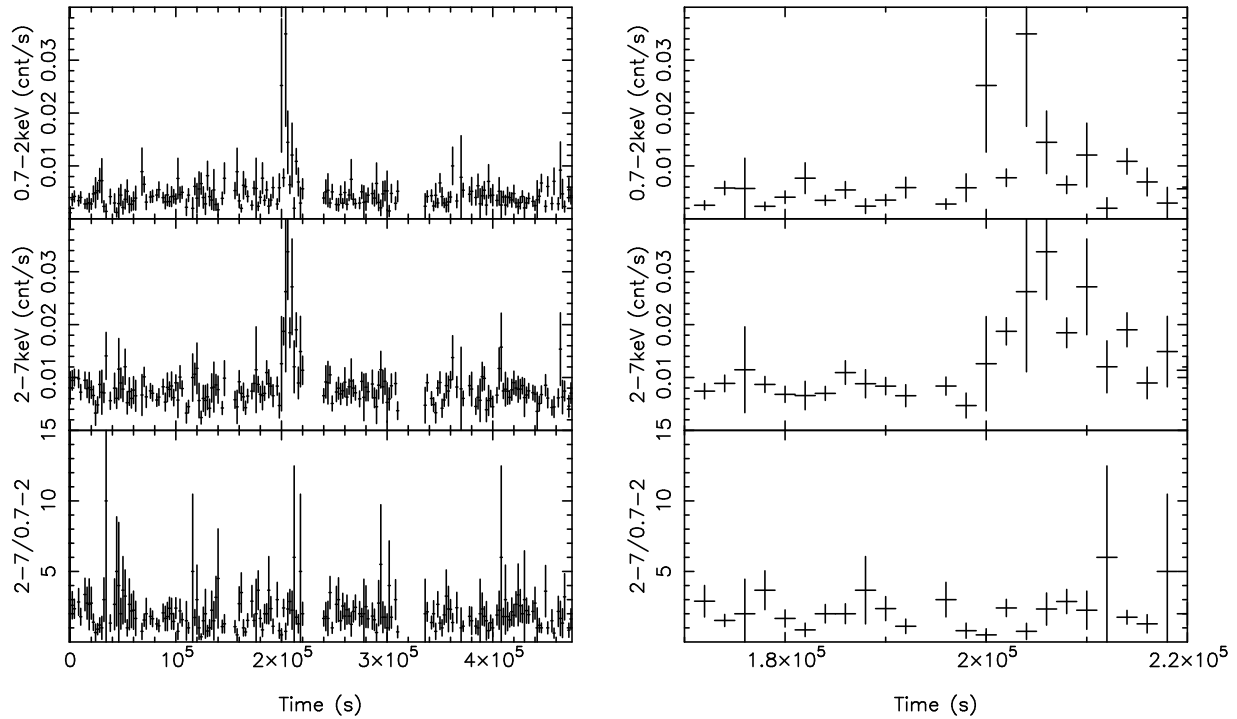


Fig. 8. Light curves of RX J0047.3–7312 (IKT1) in obs. Q with a bin time of 2000 s. The upper and middle panels present the light curves in the soft (0.7–2.0 keV) and hard (2.0–7.0 keV) bands, respectively. The lower panels present the ratio of the two bands. A flare-like activity is found at the time $\sim 2 \times 10^5$ s; the right panel shows the time zone around the flare.

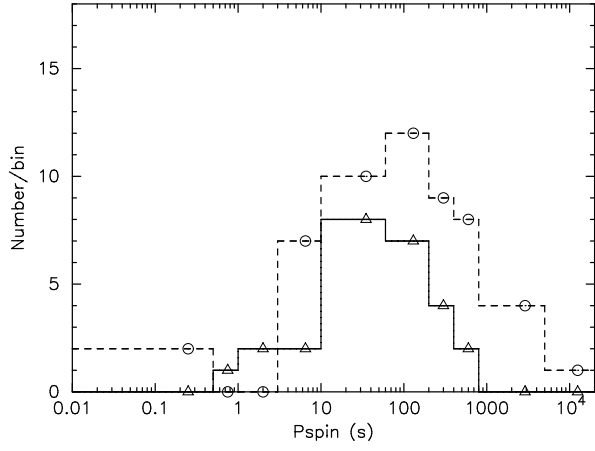


Fig. 9. Period distribution of XBPs in the SMC (solid line; triangles) and our Galaxy (dashed line; circles). The horizontal and vertical axes, respectively, indicate the pulse period and the number of XBPs in each period bin.

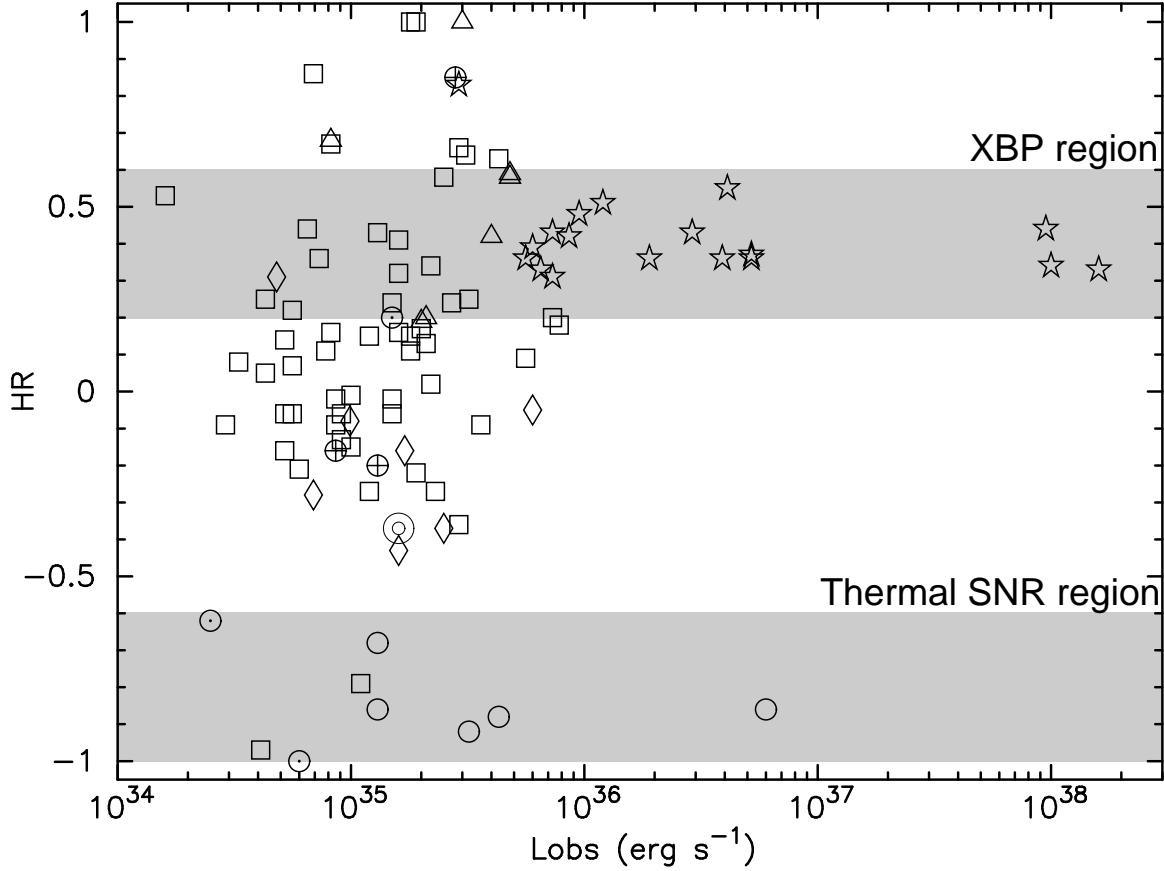


Fig. 10. Plot of HR against L_{obs} (0.7–10.0 keV) for all classes of sources in the SMC. The symbols represent XBPs (stars), thermal SNRs (circles), nonpulsating HMXBs and their candidates (triangles), radio SNRs not regarded as thermal (circles with dots), pulsars not regarded as XBPs or AXPs (circles with a plus sign), AXP (double circle), sources coincident with AGN and foreground stars (diamonds), and other unclassified sources (squares). Sources detected multiple times are represented by single points, which correspond to the largest L_{obs} of each source. HR errors for the unclassified sources are mostly $\sim \pm 0.2$. Almost all XBPs and thermal SNRs fall in the “XBP region” and “thermal SNR region”, respectively.

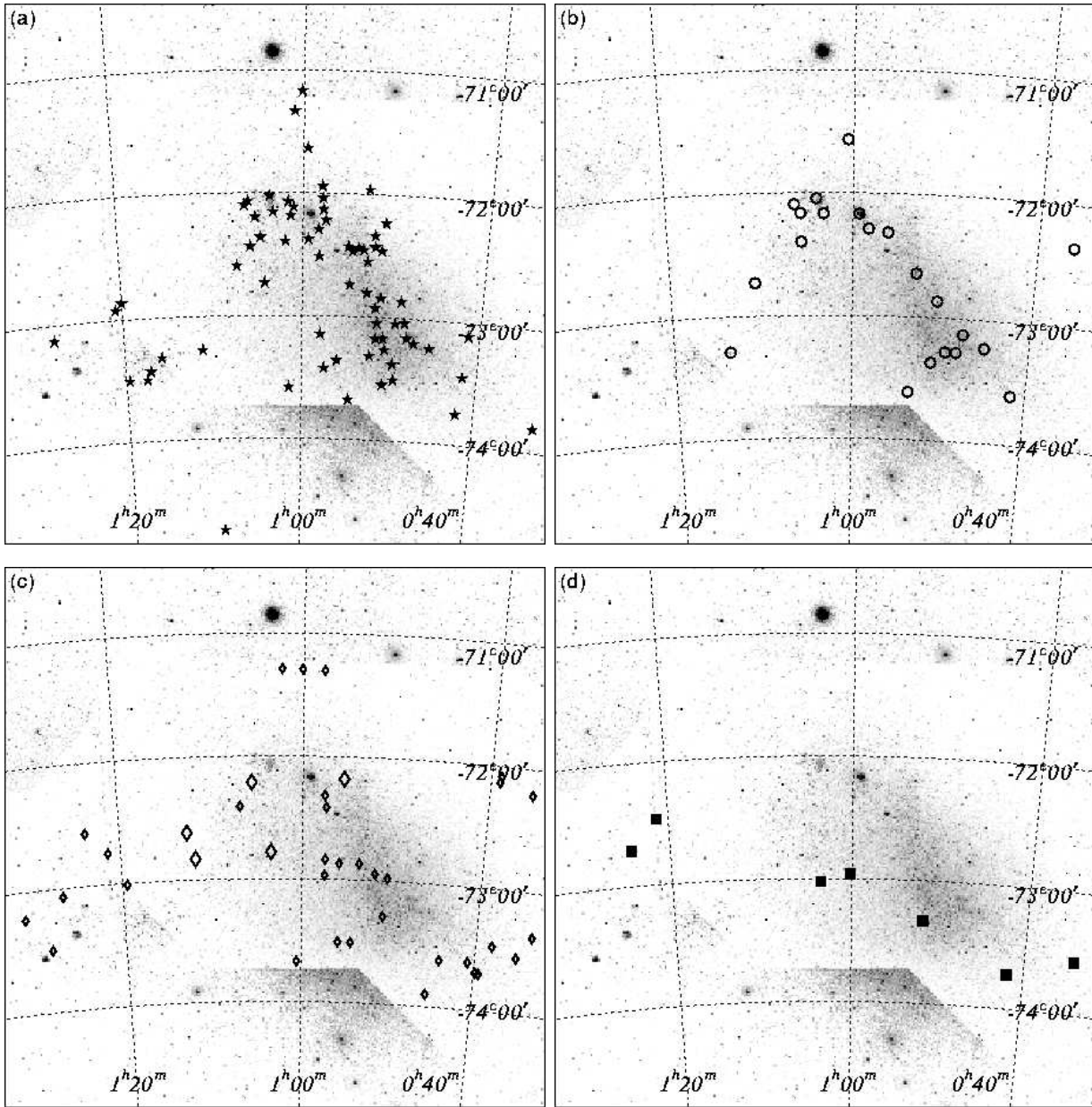


Fig. 11. Spatial distribution of HMXBs (a: indicated by stars), SNRs (b: circles), and the six AGN candidates and the 33 medium HR sources (c: diamonds), and the seven very hard sources (d: squares), superimposed on the DSS image of the SMC. The large and small diamonds in (c) indicate the AGN and the medium HR sources, respectively. The discontinuity seen in the DSS image is an artifact. The equatorial coordinates in an equinox 2000 are overlaid.

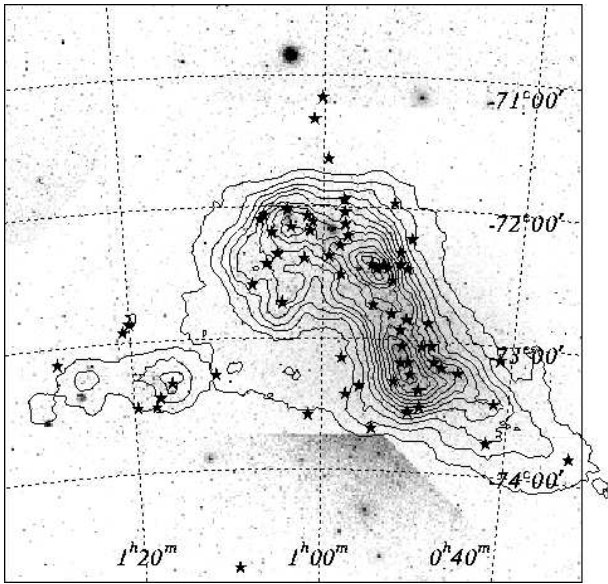


Fig. 12. Spatial distribution of HMXBs (figure 11a) superimposed on the isodensity map of young stars with ages of $(1.2-3) \times 10^7$ yr (contours; taken from Maragoudaki et al. 2001). The discontinuity seen in the DSS image is an artifact. The equatorial coordinates in an equinox 2000 are overlaid.

Table 1. ASCA observations of the SMC region.

Obs. ID	Observation date (UT)		Target name	Pointed direction (J2000)		Exposure (ks)
	Start	End		R.A. (^h ^m ^s)	Dec. ([°] ['] ^{''})	
A	1993/04/26 22:23	04/27 23:41	SMC X-1	1 17 04	-73 26 34	4/—
B	1993/05/12 08:01	05/13 12:26	E0102-72.2	1 04 02	-72 01 55	35/31 ^a
C	1995/10/18 18:32	10/19 21:31	SMC X-1	1 17 04	-73 26 35	41/—
D	1996/05/21 02:25	05/23 06:31	0103-72.6	1 04 52	-72 23 11	78/61 ^a
E	1997/05/21 13:01	05/22 01:31	1E 0035.4-7230	0 37 20	-72 14 14	23/—
F	1997/11/13 03:58	11/14 06:51	N19	0 47 16	-73 08 30	43/38 ^b
G	1997/11/14 06:51	11/15 08:22	N66	0 59 25	-72 10 12	39/34 ^b
H	1997/12/12 11:05	12/12 23:55	SMC X-3	0 52 06	-72 26 06	20/—
I	1998/11/18 17:37	11/19 15:11	XTE J0111.2-7317	1 11 26	-73 25 07	26/—
J	1998/11/24 09:39	11/25 10:51	SMC Center	0 56 05	-72 52 12	27 ^c /—
K	1999/05/10 10:31	05/11 14:00	SMC 1	0 42 06	-73 43 53	40/—
L	1999/05/11 13:59	05/12 16:46	SMC 2	0 54 44	-73 30 00	32/—
M	1999/05/12 23:11	05/14 00:35	SMC 3	1 03 33	-73 00 00	30/—
N	1999/05/14 00:35	05/15 01:56	SMC 4	1 12 08	-72 47 47	41/—
O	1999/05/28 13:24	05/29 15:11	SMC 5	1 28 36	-73 30 03	29 ^d /—
P	2000/04/04 00:09	04/07 01:30	SMC SW N1	0 42 35	-73 40 30	93/—
Q	2000/04/11 18:50	04/17 12:11	SMC SW N2	0 47 30	-73 09 13	177/96 ^b
R	2000/04/25 12:09	04/26 14:21	SMC 9	0 58 20	-73 35 00	27/—
S	2000/04/26 14:20	04/27 16:40	SMC 6	0 33 00	-73 45 00	45/—
T	2000/04/27 16:40	04/28 19:01	SMC 7	0 53 30	-71 54 00	44/—
U	2000/04/28 19:01	04/29 21:31	SMC 8	1 00 00	-71 20 00	45/—
V	2000/04/29 21:30	05/01 00:01	SMC 10	1 20 00	-72 50 00	38/—

a, b: SIS was operated in 1-CCD mode (a) or 2-CCD mode (b).

c, d: GIS was operated with a special bit assignment of 8-6-6-5-6 (c) or 8-8-8-5-2 (d), in which the time resolution was increased by a factor of 64 (c) or 4 (d), at the sacrifice of a reduction of energy resolution by a factor of 4 (c and d) and a reduction of spatial resolution by a factor of 4 (c).

Table 2. ASCA counterparts for ROSAT sources selected with the conservative criteria.

— ROSAT ^a —		— ASCA ^b —					
No.	Error ($''$)	No.	Obs. ID	Off-axis ($'$)	Sep ^c ($''$)		Remarks
34	1.8	32	F	17.0	31.9	Be-XBP	AX J0051–733 ($P = 323$ s)
34	1.8	32	Q	9.7	24.0	Be-XBP	AX J0051–733 ($P = 321$ s)
37	2.6	37	H	17.2	45.5	Be-XBP	AX J0051–722 ($P = 91$ s)
38	2.7	36	Q	14.3	40.2	SNR	0049–736
41	1.5	40	Q	11.7	32.6	Be-XBP	AX J0051.6–7311 ($P = 172$ s)
46	3.0	44	T	8.1	19.2	Be-XBP	XTE J0054–720 ($P = 167$ s)
51	2.4	47	H	10.3	10.7	Be-XBP	1WGA J0053.8–7226 ($P = 46$ s)
58	2.6	51	G	21.9 ^e	67.1	Be-XBP	XTE J0055–724 ($P = 58$ s)
73	6.4	61	G	11.6	29.8	Be-XBP?	AX J0058–7203 ($P = 280$ s)
82	4.0	66	G	3.5	4.8	SNR	0057–7226
101	3.8	78	D	9.4	11.1	Be-XBP	1SAX J0103.2–7209 ($P = 348$ s)
107	3.3	81	B	6.7	23.7	SNR	0102–723
107	3.3	81	D	16.0	14.3	SNR	0102–723
109	3.6	82	D	5.2	10.8	SNR	0103–726
118	0.7	94	A	6.9	33.6	XBP (supergiant)	SMC X-1 ($P = 0.70$ s)
118	0.7	94	C	5.3	33.8	XBP (supergiant)	SMC X-1 (eclipse)
118	0.7	94	I	23.5 ^e	35.9	XBP (supergiant)	SMC X-1 ($P = 0.70$ s)
413 ^d	6.8 ^d	21	F	3.4	27.4 ^d	SNR	0045–734
413 ^d	6.8 ^d	21	Q	6.4	36.8 ^d	SNR	0045–734

Note. — “Be-XBP” indicates an XBP with a Be star counterpart.

a: Source number and error radius of the ROSAT source presented by the HRI catalogue (Sasaki et al. 2000). The last two lines are from the PSPC catalogue (Haberl et al. 2000).

b: Source number, observation ID, and off-axis angle of the ASCA counterpart (table 5).

c: Separation angle between the ROSAT and ASCA sources.

d: The position of the ROSAT source was assumed to be the central point of No. 413 and No. 419 in Haberl et al. (2000), because SNR 0045–734 is catalogued as those two sources due to its extended X-ray emission. The error radius of the ROSAT source was taken from No. 413, while that for No. 419 is smaller, $4''7$.

e: Detected in the outer ring of the GIS.

Table 3. ASCA sources detected in multiple observations.

No.	Obs. ID ₁	Off-axis ₁ ($'$)	Obs. ID ₂	Off-axis ₂ ($'$)	Sep. ($''$)	Class	Remarks
21	Q	6.4	F	3.4	56.9	a	SNR 0045–734
32	F	17.0	Q	9.7	19.1	a	Be-XBP AX J0051–733
56	L	11.5	R	7.3	31.0	a	XBP AX J0057.4–7325
81	D	16.0	B	6.7	26.8	a	SNR 0102–723
94	I	23.5 ^a	A	6.9	32.4	a	XBP (supergiant) SMC X-1
25	F	9.7	Q	4.2	16.5	b	SNR 0047–735
36	F	19.2 ^a	L	16.9	70.0	b	SNR 0049–736
36	F	19.2 ^a	Q	14.2	59.4	b	SNR 0049–736
36	L	16.9	Q	14.2	53.2	b	SNR 0049–736
94	I	23.5 ^a	C	5.3	33.4	b	XBP (supergiant) SMC X-1
94	A	6.9	C	5.3	1.0	b	XBP (supergiant) SMC X-1
17	P	4.3	K	2.7	21.7	c	Pulsar AX J0043–737
20	Q	7.5	F	2.7	19.6	c	Be-XBP? RX J0047.3–7312 (IKT1)
24	F	22.1 ^a	H	21.7 ^a	72.1	c	Be-XBP AX J0049–729
24	F	22.1 ^a	Q	17.4	34.5	c	Be-XBP AX J0049–729
24	H	21.7 ^a	Q	17.4	57.3	c	Be-XBP AX J0049–729
30	L	20.7 ^a	F	16.3	48.9	c	Be-XBP? AX J0049.5–7323
30	F	16.3	Q	13.7	53.8	c	Be-XBP? AX J0049.5–7323
30	L	20.7 ^a	Q	13.7	39.9	c	Be-XBP? AX J0049.5–7323
40	F	20.9 ^a	L	20.7 ^a	31.8	c	Be-XBP AX J0051.6–7311
40	F	20.9 ^a	Q	11.7	53.7	c	Be-XBP AX J0051.6–7311
40	L	20.7 ^a	Q	11.7	53.7	c	Be-XBP AX J0051.6–7311
61	T	22.6 ^a	G	11.6	69.0	c	Be-XBP? AX J0058–7203
74	B	18.4	D	17.0	47.1	c	Be-XBP RX J0101.3–7211
74	D	17.0	G	10.4	19.0	c	Be-XBP RX J0101.3–7211
74	B	18.4	G	10.4	54.5	c	Be-XBP RX J0101.3–7211
78	B	13.9	D	11.1	18.4	c	Be-XBP 1SAX J0103.2–7209
78	G	19.0	D	11.1	20.0	c	Be-XBP 1SAX J0103.2–7209
78	G	19.0	B	13.9	25.8	c	Be-XBP 1SAX J0103.2–7209
22	F	6.0	Q	3.3	25.7	d	
26	F	10.5	Q	2.6 ^b	38.7	d	
28	L	21.2 ^a	F	21.0 ^a	48.6	d	
28	L	21.2 ^a	Q	20.9 ^a	68.7	d	
52	T	21.9 ^a	G	15.6	63.0	d	
53	R	10.9	L	4.7	55.5	d	
76	G	16.1	D	14.3	14.1	d	

Note. — Columns 1–6 give the source number, the observation IDs and off-axis angles for multiple detections, and the separation angle between the positions in the two observations. Off-axis angles are sorted so that off-axis₁ is larger than off-axis₂. “Be-XBP” indicates an XBP with a Be star counterpart.

a: Detected in the outer ring of the GIS.

b: Detected with the SIS.

Table 4. X-Ray pulsars in the SMC.

No.	Names	Period ^a (s)	Optical ID	References
17	AX J0043–737 ^b	0.08758073(4)	...	1
20	RX J0047.3–7312	[263(1)] ^c	Be?	2
24	AX J0049–729	74.68(2)	Be	3, 4, 5, 6
26	AX J0049–732	9.1320(4)	... ^d	7, 8, 9
30	AX J0049.5–7323	755.5(6)	Be?	2, 10, 11
...	XTE J0050–732#1	[16.6]	...	12
...	XTE J0050–732#2	[25.5]	...	12
32	AX J0051–733	323.2(5) - obs. F 321.0(1) - obs. Q	Be	6, 13, 14, 15
37	AX J0051–722	91.12(5)	Be	3, 5, 16
40	AX J0051.6–7311	172.40(3)	Be	15, 17, 18
...	2E 0050.1–7247	[8.8816(2)]	Be	5, 19
...	XTE J0052–723	[4.782(1)]	...	20
...	XTE J0052–725	[82.4(2)]	...	21
...	46.4-s pulsar	[46.4(1)]	...	21
43	RX J0052.1–7319	[15.3(1)]	Be	22, 23, 24
...	XTE SMC95	[95]	...	25
44	XTE J0054–720	167.8(2)	Be	15, 26, 27
47	1WGA J0053.8–7226	46.63(4)	Be	3, 28
49	SMC X-2	2.37230(4)	Be	29, 30, 31, 32
51	XTE J0055–724	[58.963(3)]	Be	5, 6, 33, 34, 35
56	AX J0057.4–7325	101.45(7) - obs. R 101.47(6) - obs. L	...	30, 36
61	AX J0058–7203	280.4(4)	Be?	2, 13, 37
67	RX J0059.2–7138	2.763221(4) ^e	Be	38, 39, 40
72	CXOU J0110043.1–721134	[5.44]	...	41
74	RX J0101.3–7211	[455(2)]	Be	42
78	1SAX J0103.2–7209	348.9(3)	Be	6, 43, 44, 45
83	AX J0105–722 ^b	3.34300(3)	... ^d	46, 47
90	XTE J0111.2–7317	30.9497(4)	Be	23, 48, 49, 50
94	SMC X-1	0.70865(6) - obs. A 0.7065(5) - obs. I	B (SG ^f)	51, 52
...	RX J0117.6–7330	[22.0669(1)]	Be	53, 54

Note. — Pulsars are sorted in order of the right ascension of each source. Most of the pulsars in this table are regarded as XBPs, except for AX J0043–737, AX J0049–732, and AX J0105–722 (see subsection 5.1). References — (1) Yokogawa and Koyama (2000); (2) Haberl and Sasaki (2000); (3) Corbet et al. (1998); (4) Yokogawa et al. (1999); (5) Stevens et al. (1999); (6) Coe and Orosz (2000); (7) Imanishi et al. (1998); (8) Ueno et al. (2000a); (9) Filipović et al. (2000a); (10) Ueno et al. (2000b); (11) Yokogawa et al. (2000a); (12) Lamb et al. (2002a); (13) Yokogawa and Koyama (1998a); (14) Imanishi et al. (1999); (15) Cowley et al. (1997); (16) Ozaki et al. (2000); (17) Torii et al. (2000a); (18) Yokogawa et al. (2000b); (19) Israel et al. (1997); (20) Corbet et al. (2001a); (21) Corbet et al. (2002); (22) Lamb et al. (1999); (23) Israel et al. (1999); (24) Kahabka (2000); (25) Laycock et al. (2002); (26) Lochner et al. (1998); (27) Yokogawa et al. (2001a); (28) Buckley et al. (2001); (29) Corbet et al. (2001b); (30) Torii et al. (2000b); (31) Yokogawa et al. (2001b); (32) Murdin et al. (1979); (33) Marshall and Lochner (1998); (34) Santangelo et al. (1998); (35) Israel et al. (1998b); (36) Yokogawa et al. (2000c); (37) Tsujimoto et al. (1999); (38) Hughes (1994); (39) Kohno et al. (2000); (40) Southwell and Charles (1996); (41) Lamb et al. (2002b); (42) Sasaki et al. (2001); (43) Israel et al. (2000); (44) Hughes and Smith (1994); (45) Ye et al. (1995); (46) Yokogawa and Koyama (1998b); (47) Filipović et al. (2000b); (48) Chakrabarty et al. (1998a); Wilson and Finger (1998); (49) Yokogawa et al. (2000d); (50) Coe et al. (2000); (51) Lucke et al. (1976); (52) Petro et al. (1973); (53) Coe et al. (1998); (54) Macomb et al. (1999)

a: The periods determined in this work are presented with the error for the last digit in parentheses. Correction for the orbital Doppler effect was carried out only for SMC X-1. Periods in square brackets were determined by others and not detected in this work.

b: Pulsations detected with low significance. See subsections 5.1.1 and 5.1.20.

c: See subsection 5.1.2.

d: AX J0049–732 and AX J0105–722 were once identified with ROSAT sources RX J0049.4–7310 and RX J0105.1–7211 (Filipović et al. 2000a, 2000b), respectively. Since these ROSAT sources have emission line objects as counterparts, it was previously proposed that AX J0049–732 and AX J0105–722 were Be/X-ray binaries. However, according to the improved positions determined in this study, the identification with the ROSAT sources is now a little questionable (see table 5, subsections 5.1.4, and 5.1.20).

e: Determined by a detailed pulse phase analysis (Kohno et al. 2000).

f: A supergiant (B0 I), Sk 160.

Table 5. ASCA catalogue of discrete X-ray sources in the SMC region.

No. ^a	Coordinates (J2000)		Det. ^b	S/N	PSPC ^d		HRI ^e		IPC ^f		Class ^g	Names ^h	Comments ⁱ
	R.A.	Dec.			Y/N	No.	Sep.	No.	Sep.	No.			
	(^h ^m ^s)	([°] ['] ^{''})			(^{''})	(^{''})	(^{''})	(^{''})	(^{''})	(^{''})			
1*	0 33 44.3	-73 21 41	S/	12.4	462	14					UN(m)		
2*	0 34 05.4	-73 31 30	S/	7.1							UN		
3*	0 34 19.4	-73 33 57	S/	27.8							UN(h)		
4*	0 35 18.3	-73 32 42	S/	9.1	518	43					UN(m)		
5*	0 35 28.0	-72 12 43	E/	7.2	167	31	2	31			UN(m)		
6*	0 36 09.2	-72 21 05	E/	8.2	211	34	4	34			TSc		fg star ¹ ; AGN? ²
7*	0 38 09.9	-73 27 54	P/K	13.3							UN(m)		
8*	0 38 56.5	-72 04 53	E/	7.8	127	47	9	45			UN(m)		
9*	0 39 03.1	-72 07 49	E/	7.1							UN(m)		
10*	0 39 27.3	-73 41 58	P/K	7.6							UN(m)		
11*	0 39 52.0	-73 41 36	K/P	10.5							UN(m)		
12*	0 40 46.4	-73 36 58	P/K	6.4							UN(m)		
13*	0 41 29.9	-73 36 37	P/K	6.0							UN		
14*	0 41 37.0	-73 26 47	P/K	6.6	481	30					BPc		
15*	0 41 57.9	-73 43 22	K/P	9.7							UN(h)		
16*	0 42 04.8	-73 44 58	P/K	16.2			11	16			BPc		
17*	0 42 39.9	-73 40 25	KP/	10.4	546	17	12	18			P	AX J0043-737	$P = 87$ ms? (obs. K); XB? or AGN? ²
18*	0 44 06.6	-73 37 03	P/K	17.0							UN(m)		
19 [†]	0 45 25.6	-73 53 55	P/K	10.1							UN(m)		
20*	0 47 22.9	-73 12 06	QF/	60.1	434	18			18	55	BP	RX J0047.3-7312; IKT1	[$P = 263$ s]; Be/X? ³ ; flare (obs. Q)
21*	0 47 30.0	-73 08 25	QF/	39.6	413	37 ^k			16	38	TS	SNR 0045-734; N19; DEM S32; IKT2	old, overabundant, center-filled
22*	0 48 14.0	-73 09 39	QF/	52.5					20	47	NHc, BPc	AX J0048.2-7309	Be/X? (§5.3.1); Fe line? (obs. Q)
23*	0 48 37.6	-73 18 59	Q/F	6.1	454	60			21	49	RS, TSc	SNR 0046-735; N22; DEM S37; IKT4	

Table 5. (Continued)

No. ^a	Coordinates (J2000)		Det. ^b	S/N	PSPC ^d		HRI ^e		IPC ^f		Class ^g	Names ^h	Comments ⁱ
	R.A.	Dec.			Y/N	No.	Sep.	No.	Sep.	No.			
	(^h ^m ^s)	([°] ['] ^{''})			(^{''})	(^{''})	(^{''})	(^{''})	(^{''})	(^{''})			
24 [†]	0 49 01.6	-72 51 46	FQH/	71.4	351	54					BP	AX J0049-729; RX J0049.1-7250	$P = 74$ s; Be/X
25*	0 49 08.3	-73 13 21	QF/	11.7	437	45		22	47		RS,TSc	SNR 0047-735; DEM S49; IKT5	
26*	0 49 18.5	-73 12 01	FQ/	11.7	430	33					P	AX J0049-732; RX J0049.0-7314	$P = 9.13$ s
27*	0 49 26.3	-73 10 51	Q/F	17.9	427	50					UN	RX J0049.4-7310	Be/X? ³ ; pos. and spec. from SIS
28 [†]	0 49 32.0	-73 30 17	LFQ/	12.3	511	68	28	52			NHc,BPc	RX J0049.5-7331	Be/X? ³
29*	0 49 35.2	-73 02 47	Q/F	8.8							BPc		
30*	0 49 42.8	-73 22 40	QFL/	19.5	468	22					BP	AX J0049.5-7323; RX J0049.7-7323	$P = 755$ s; Be/X? ³
31*	0 50 28.8	-72 58 35	Q/F	6.0							UN(m)		
32*	0 50 40.5	-73 15 46	QF/L	208.8	444	20	34	24			BP	AX J0051-733; RX J0050.8-7316	$P = 323$ s; Be/X; brightened (obs. Q)
33*	0 50 45.4	-72 41 57	H/	11.3			35	18			FS		fg star SkKM 62 ²
34 [†]	0 50 50.7	-73 17 16	L/F ^j Q ^j	7.9							UN(m)		
35*	0 50 53.5	-73 10 07	Q/F	40.4	421	13	36	16			NHc,BPc	RX J0050.9-7310	Be/X? ³
36*	0 50 58.1	-73 20 55	QFL/	39.7	461	50	38	40	24	43	TS	SNR 0049-736; IKT6	
37*	0 51 06.4	-72 13 58	H/	52.0			37	46			BP	AX J0051-722	$P = 91$ s; Be/X
38*	0 51 25.4	-72 27 29	H/	8.5							BPc		
39*	0 51 39.9	-73 02 58	Q/F	9.0							BPc		
40*	0 51 44.5	-73 10 34	QFL/	36.2	424	31	41	33	25	31	BP	AX J0051.6-7311; RX J0051.9-7311; IKT7	$P = 172$ s; Be/X
41*	0 51 55.7	-72 56 49	Q/	5.9							UN(m)		
42*	0 51 56.2	-73 19 39	Q/L	7.7					29	47	UN(h)		
43 [†]	0 52 22.1	-73 19 05	F/LQ	5.2	453	36	44	38	29	71	BP	RX J0052.1-7319; IKT8	[$P = 15$ s]; Be/X
44*	0 52 58.4	-71 57 54	T/	38.1	94	19	46	19	32	48	BP	XTE J0054-720; AX J0052.9-7157; RX J0052.9-7158; IKT9	$P = 167$ s; Be/X
45*	0 53 29.2	-73 36 40	L/R	5.8							TSc		
46*	0 53 42.1	-72 52 12	J/	8.8							UN(m)		

Table 5. (Continued)

No. ^a	Coordinates (J2000)		Det. ^b	S/N	PSPC ^d		HRI ^e		IPC ^f		Class ^g	Names ^h	Comments ⁱ
	R.A.	Dec.			Y/N	No.	Sep.	No.	Sep.	No.			
	(^h ^m ^s)	([°] ' ")			(")	(")	(")						
47*	0 53 55.2	-72 26 42	H/	94.8	242	21	51	11	34	15	BP	1WGA J0053.8-7226; XTE J0053-724; IKT10	$P = 46$ s; Be/X
48*	0 54 25.1	-73 30 32	L/R	5.7							UN(m)		
49*	0 54 36.2	-73 40 35	R/L	69.7	547	31					BP	SMC X-2	$P = 2.37$ s; Be/X; Fe line
50*	0 54 49.4	-72 44 23	J/	15.0	324	50	57	52			NHc,BPc	RX J0054.9-7245	Be/X? ³
51 [†]	0 55 01.6	-72 25 49	G/	16.9	241	64	58	67	35	43	BP	XTE J0055-724; 1SAX J0054.9-7226; IKT11	[$P = 58$ s]; Be/X
52*	0 55 36.1	-72 10 56	GT/	20.5	157	41	59	34	36	20	AGN		AGN? ¹
53*	0 55 51.6	-73 30 32	LR/	12.7	508	33	65	35			UN(m)		
54*	0 55 55.5	-72 52 15	J/	9.1			66	31			UN(m)		
55*	0 57 27.2	-72 25 01	G/	5.1	234	48			39	51	UN(m)	IKT14	
56*	0 57 28.6	-73 25 29	RL/	43.9	476	28	70	14			BP	AX J0057.4-7325	$P = 101$ s; probably an XBP
57*	0 57 28.7	-72 50 17	J/	11.7							UN(m)		
58*	0 57 29.3	-72 58 08	J/	9.0							UN(m)		
59*	0 57 37.4	-72 19 07	G/	14.0							UN(m)		
60*	0 57 54.2	-71 18 04	U/	8.5	14	28					UN(m)		
61*	0 57 54.7	-72 02 26	GT/	40.2	114	33	73	30	41	50	BP	AX J0058-7203	$P = 280$ s; Be/X? ³
62*	0 57 57.3	-73 08 55	J/	7.8							BPc		
63*	0 58 15.8	-72 30 26	G/	7.7	258	33	76	28			NH	RX J0058.2-7231	Be/X ³
64*	0 58 19.5	-72 17 40	G/	13.9	194	29	77	29	42	17	RS,BPc	SNR 0056-725; IKT16	hard spectrum
65*	0 59 24.2	-72 22 35	G/	17.9	218	44	81	47			BPc		XB? ²
66*	0 59 27.2	-72 10 03	G/	22.3	148	11	82	5	44	11	TS	SNR 0057-7226; N66; DEM S103; IKT18	old, ISM abundance, center-filled
67 [†]	0 59 35.3	-71 38 02	B/	590.0	53	122					BP	RX J0059.2-7138	$P = 2.76$ s; Be/X; at the GIS edge
68*	1 00 09.0	-71 17 37	U/	7.8	13	39					UN(m)		
69*	1 00 09.6	-72 57 36	M/	6.0			84	10			UN(h)		
70*	1 00 12.1	-71 10 15	U/	5.8							BPc		

Table 5. (Continued)

No. ^a	Coordinates (J2000)		Det. ^b	S/N	PSPC ^d		HRI ^e		IPC ^f		Class ^g	Names ^h	Comments ⁱ
	R.A.	Dec.			Y/N	No.	Sep.	No.	Sep.	No.			
	(^h ^m ^s)	(^o ' ")	(^{''})	(^{''})							(^{''})		
71*	1 00 32.8	-73 40 12	R/	18.0							UN(m)		
72*	1 00 41.1	-72 11 16	G/	14.0	162	19	90	18	45	38	AXP	CXOU J0110043.1-721134; IKT19	[$P = 5.44$ s]; [hard] ¹ ; AGN? ²
73*	1 00 58.1	-71 20 04	U/	16.6	18	21					BPc		
74*	1 01 19.6	-72 10 59	GDB/	30.0	159	22	95	19			BP	RX J0101.3-7211	[$P = 455$ s]; Be/X
75*	1 01 27.8	-73 35 00	R/	5.2							BPc		
76*	1 01 53.0	-72 23 01	DG/	12.9	220	27	97	34			NHc	RX J0101.8-7223	Be/X? ³
77*	1 02 14.6	-71 17 20	U/	5.1							UN(m)		
78*	1 03 15.3	-72 09 19	DBG/	24.7	143	7	101	9	50	23	BP	1SAX J0103.2-7209; SNR 0101-724; IKT21	$P = 348$ s; Be/X
79*	1 03 27.3	-73 01 24	M/	16.5	384	9					UN(h)		
80*	1 03 27.5	-72 46 55	M/	13.5	334	34	104	33			AGN		AGN? ²
81*	1 04 01.7	-72 01 40	BD/	317.3	107	8	107	24	51	19	TS	SNR 0102-723; N76; DEM S124; IKT22	
82*	1 05 01.2	-72 23 06	D/	64.5	217	14	109	11	52	42	TS	SNR 0103-726; DEM S125; IKT23	old, overabundant, center-filled+shell
83*	1 05 07.6	-72 10 34	D/B	23.3							RS,P	AX J0105-722	$P = 3.34$ s?; multiple sources (§5.1.20)
84*	1 05 30.1	-72 12 47	D/B	15.1	172	46	112	45			AGN		[nonstar] ¹ ; AGN? ²
85*	1 05 52.1	-72 03 41	D/B	6.9	120	18					NHc	RX J0105.9-7203	Be/X? ³ ; contamination from No. 81
86*	1 06 48.5	-72 24 32	D/	14.5	230	41	116	44	55	66	UN(m)	DEM S134	[hard] ¹
87 [†]	1 07 13.5	-72 34 39	D/	5.6	279	58			56	46	NHc	RX J0107.1-7235	Be/X? ³
88 [†]	1 07 27.2	-72 43 26	N/	4.7	313	9					UN		[nonstar] ¹ ; contamination from No. 89
89 [†]	1 07 39.5	-72 42 15	N/	10.0	307	72					UN		contamination from No. 88
90*	1 11 10.1	-73 16 32	I/A	4869.6	446	41					BP	XTE J0111.2-7317	$P = 30$ s; Be/X; Fe line
91*	1 11 45.8	-72 49 52	N/	6.1	348	42					AGN		AGN $z = 0.197^1$
92*	1 12 38.7	-72 36 51	N/	7.3	283	55					AGN		AGN $z = 1.376^1$
93*	1 13 05.5	-72 46 25	N/	6.9	330	26					BPc		
94*	1 17 08.5	-73 26 07	ACI/	357.8	482	28	118	34	63	13	BP	SMC X-1	$P = 0.70$ s; HMXB, supergiant (B0I)

Table 5. (Continued)

No. ^a	Coordinates (J2000)		Det. ^b	S/N	PSPC ^d		HRI ^e		IPC ^f		Class ^g	Names ^h	Comments ⁱ
	R.A.	Dec.			Y/N	No.	Sep.	No.	Sep.	No.			
	(^h ^m ^s)	([°] ['] ^{''})			(^{''})	(^{''})	(^{''})	(^{''})	(^{''})	(^{''})			
95*	1 18 37.9	-73 25 22	C/A ⁱ	22.5	478	4	120	5	65	13	FS		fg star G5 V, HD 8191
96*	1 19 27.3	-73 00 51	V/	13.1	385	39			66	20	UN(m)		cluster $z = 0.0656^1$
97*	1 20 01.0	-72 51 46	V/	8.8							BPc		
98*	1 20 44.5	-72 55 13	V/	8.5							BPc		
99*	1 21 16.2	-72 27 42	V/	7.7							UN(h)		
100*	1 21 23.9	-72 44 53	V/	25.7	316	55					UN(m)		
101*	1 23 44.6	-72 34 26	V/	9.1	275	44					UN(m)		
102*	1 24 15.7	-72 42 32	V/	13.0							UN(h)		
103 [†]	1 26 44.2	-73 04 20	O/	15.3							UN(m)		in stray light
104*	1 27 48.0	-73 07 39	O/	16.9							BPc		in stray light
105*	1 28 28.6	-73 29 46	O/	12.9				67	35		UN(m)	AX J0128.4-7329	center of a supergiant shell, SMC-1
106*	1 31 12.0	-73 13 44	O/	6.8							UN(m)		

a: Source number. Sources with “*” were detected in the inner circle of the GIS and have an error radius of $\sim 40''$ at 90% confidence (subsection 3.3.1). Sources with “†” were detected in the outer ring of the GIS and their error radius is larger.

b: Y and N represent observation IDs (table 1) when the source was detected and not detected, respectively. For sources detected multiple times, the first ID in this column was used to determine its position.

c: The largest value of S/N for each source. The criterion of source detection is $S/N > 5$.

d: Counterpart found in the ROSAT PSPC catalogue (Haberl et al. 2000). Source number and separation (in arcsec) from the ASCA source are given.

e: The same as c, but for the ROSAT HRI catalogue (Sasaki et al. 2000).

f: The same as c, but for the Einstein IPC catalogue (Wang, Wu 1992).

g: Source class (see subsection 6.2.1): TS (thermal SNRs; subsection 4.2.3), RS (radio SNRs which are not classified as a thermal SNR), TSc (thermal SNR candidates; subsection 6.2.3), BP (X-ray binary pulsars; subsection 5.1), BPc (candidates of X-ray binary pulsar; subsection 6.2.3), AXP (anomalous X-ray pulsar), P (the remaining pulsars), NH (non-pulsating HMXBs; table 8), AGN (sources coincident with an AGN), FS (sources coincident with a foreground star), and UN (unclassified sources).

h: Source names usually used in the literature. References for the abbreviations are Davies et al. (1976) for DEM’s, Inoue et al. (1983) for IKT’s, Henize (1956) for N’s, and Mathewson et al. (1983, 1984) for SNR’s.

i: Periods in square brackets were determined by others and not detected in this work (see also table 4). References for comments with superscripts 1, 2, and 3 are Haberl et al. (2000), Sasaki et al. (2000), and Haberl and Sasaki (2000), respectively.

j: In these observations, nearby sources were too bright, thus detection of No. 34 and No. 95 was hampered.

k: The separation angle from the central point of No. 413 and 419 in Haberl et al. (2000).

Table 6. Spectral parameters of the ASCA sources.

No.	HR ^a	Obs. ID ^b	Γ^c	kT^c	N_{H}^c	F_{X}^d	L_{obs}^d	L_{X}^d
1	-0.27±0.14	S	2.5 (1.7–4.6)		2 (<15)	0.53	0.23	0.29
2	-1.00±2.00	S
3	0.64±0.09	S	1.8 (1.0–3.0)		47 (17–100)	0.72	0.31	0.65
4	-0.13±0.18	S	1.9 (1.2–3.7)		0 (<7)	0.21	0.091	0.091
5	-0.27±0.24	E	2.1 (1.0–5.3)		3 (<22)	0.28	0.12	0.15
6	-0.79±0.35	E	3.6 (>2.2)		2 (<37)	0.25	0.11	0.16
6	-0.79±0.35	E		1.1 (0.1–2.5)	0 (<20)	0.23	0.099	0.099
7	0.02±0.12	P	1.4 (1.0–2.0)		0 (<0.5)	0.52	0.22	0.22
8	0.16±0.23	E	1.8 (0.7–4.2)		7 (<46)	0.19	0.082	0.11
9	-0.16±0.25	E	2.2 (1.3–5.2)		0 (<20)	0.12	0.052	0.052
10	-0.02±0.20	P	1.2 (0.5–5.1)		0 (<69)	0.20	0.086	0.086
11	-0.15±0.16	K	2.0 (1.4–3.5)		0 (<6)	0.24	0.10	0.10
12	-0.09±0.24	P	2.1 (1.3–4.4)		0 (<31)	0.066	0.029	0.029
13	-1.00±1.15	P
14	0.22±0.23	P	2.1 (0.8–4.2)		9 (<31)	0.13	0.056	0.086
15	0.86±0.25	K	3.9 (2.2–7.0)		57 (23–120)	0.16	0.069	1.2
16	0.43±0.10	P	1.8 (0.9–2.9)		18 (0.7–39)	0.31	0.13	0.22
17	-0.16±0.15	K	1.7 (1.3–2.4)		0 (<4)	0.20	0.086	0.086
17		P				0.11	0.048	0.048
18	0.15±0.10	P	2.2 (1.3–3.6)		11 (0.6–28)	0.27	0.12	0.20
19	0.13±0.15	P	1.5 (0.9–2.5)		0 (<6)	0.48	0.21	0.21
20	0.39±0.03	F	1.0 (0.9–1.2)		4 (1–7)	0.67	0.29	0.32
20		Q				1.4	0.60	0.65
21	-0.86±0.06	F		0.37 (0.32–0.47)	10 (8–11)	0.29	0.13	1.3
21		Q				0.29	0.13	1.3
22	0.59±0.05	F	0.8 (0.6–1.1)		9 (3–17)	0.20	0.086	0.099

Table 6. (Continued)

No.	HR ^a	Obs. ID ^b	Γ^c	kT^c	N_{H}^c	F_{X}^d	L_{obs}^d	L_{X}^d
22		Q				1.1	0.48	0.52
23	-0.62±0.36	Q		0.9 (0.1–1.8)	0 (<15)	0.058	0.025	0.025
24	0.36±0.03	F	1.0 (0.8–1.1)		3 (2–5)	12	5.2	5.5
24		H				1.6	0.69	0.76
24		Q				0.71	0.31	0.33
25	-1.00±1.38	F		0.86 (0.82–0.90)	0 (<0.4)	0.14	0.060	0.060
25		Q				0.11	0.048	0.048
26	0.85±0.20	F	0.9 (0.3–1.6)		15 (6–28)	0.64	0.28	0.33
26		Q				0.37	0.16	0.19
27	...	Q	1.7 (0.8–2.9)		27 (11–58)	0.23	0.099	0.17
28	0.58±0.12	F	0.9 (0.3–1.7)		6 (<20)	0.82	0.35	0.39
28		L				1.1	0.48	0.51
28		Q				0.84	0.36	0.40
29	0.25±0.18	Q	1.0 (0.3–1.7)		0 (<19)	0.10	0.043	0.043
30	0.31±0.06	F	0.8 (0.7–1.0)		0 (<3)	1.1	0.48	0.48
30		L				1.5	0.65	0.65
30		Q				1.7	0.73	0.73
31	0.08±0.31	Q	1.3 (-0.1–4.5)		0 (<30)	0.077	0.033	0.033
32	0.43±0.01	F	0.76 (0.69–0.83)		2.2 (1.2–3.3)	2.9	1.3	1.3
32		Q				6.8	2.9	3.0
33	-0.16±0.16	H	2.2 (1.5–3.6)		2 (<11)	0.39	0.17	0.20
34	0.09±0.20	L	0.6 (-0.4–1.6)		0 (<11)	1.3	0.56	0.56
35	0.42±0.04	Q	1.0 (0.8–1.3)		4 (0.9–8)	0.92	0.40	0.43
36	-0.92±0.07	F		0.23 (0.18–0.47)	6 (2–7)	0.64	0.28	1.8
36		L				0.65	0.28	1.8
36		Q				0.74	0.32	2.0
37	0.55±0.04	H	1.0 (0.7–1.3)		10 (5–16)	9.5	4.1	4.8

Table 6. (Continued)

No.	HR ^a	Obs. ID ^b	Γ^c	kT^c	N_{H}^c	F_{X}^d	L_{obs}^d	L_{X}^d
38	0.58±0.20	H	0.1 (−1.0–1.3)		0 (<21)	0.58	0.25	0.25
39	0.53±0.38	Q	10 (>2.7)		140 (95–200)	0.038	0.016	... ^e
40	0.33±0.04	F	0.9 (0.8–1.0)		0 (<0.8)	0.68	0.29	0.29
40		L				1.5	0.65	0.65
40		Q				1.3	0.56	0.56
41	0.05±0.32	Q	1.8 (0.5–5.5)		0 (<43)	0.10	0.043	0.043
42	0.67±0.29	Q	3.3 (1.2–7.1)		6 (1–16)	0.19	0.082	0.78
43	0.83±0.36	F	2.9 (...)		53 (<290)	0.68	0.29	1.6
44	0.42±0.05	T	0.7 (0.5–1.0)		0.7 (<5)	2.0	0.86	0.88
45	−0.97±0.51	L	5.1 (>2.4)		9 (<45)	0.093	0.040	0.29
45	−0.97±0.51	L		0.6 (0.2–2.1)	10 (<31)	0.096	0.041	0.41
46	−0.06±0.18	J	4.0 (1.8–8.9)		27 (0.7–92)	0.21	0.091	0.86
47	0.37±0.02	H	0.8 (0.7–0.9)		1 (<2)	12	5.2	5.2
48	−0.06±0.27	L	1.3 (0.2–4.1)		0 (<14)	0.12	0.052	0.052
49	0.36±0.03	R	0.7 (0.5–0.9)		0 (<1)	9.1	3.9	3.9
50	0.20±0.11	J	1.8 (1.1–2.8)		6 (<19)	0.49	0.21	0.28
51	0.51±0.10	G	0.4 (0.1–1.0)		0.02 (<10)	2.7	1.2	1.2
52	−0.05±0.09	G	1.5 (1.2–1.8)		0 (<2)	0.44	0.19	0.19
52		T				1.4	0.60	0.60
53	−0.01±0.11	L	2.1 (1.6–2.7)		0 (<2)	0.21	0.091	0.091
53		R				0.24	0.10	0.10
54	0.11±0.17	J	2.4 (1.3–4.1)		11 (<36)	0.18	0.078	0.15
55	−0.06±0.31	G	5.3 (>2.1)		35 (5–110)	0.13	0.056	2.6
56	0.48±0.05	L	1.1 (0.9–1.4)		8 (4–14)	1.1	0.48	0.56
56		R				2.2	0.95	1.1
57	0.17±0.14	J	1.4 (0.9–2.4)		2 (<13)	0.47	0.20	0.22
58	−0.02±0.17	J	1.7 (1.2–3.2)		0 (<17)	0.35	0.15	0.15

Table 6. (Continued)

No.	HR ^a	Obs. ID ^b	Γ^c	kT^c	N_{H}^c	F_{X}^d	L_{obs}^d	L_{X}^d
59	0.15±0.12	G	1.6 (0.9–2.6)		4 (<15)	0.42	0.18	0.21
60	−0.09±0.18	U	2.2 (1.5–3.5)		0 (<10)	0.20	0.086	0.086
61	0.36±0.04	G	0.8 (0.6–1.0)		0.7 (<4)	2.5	1.1	1.1
61		T				4.4	1.9	1.9
62	0.24±0.20	J	1.8 (0.7–4.1)		7 (<37)	0.62	0.27	0.36
63	1.00±0.29	G	2.6 (0.2–6.0)		89 (29–230)	0.70	0.30	1.4
64	0.20±0.12	G	1.5 (1.0–2.3)		2 (<12)	0.34	0.15	0.16
65	0.25±0.09	G	1.0 (0.7–1.5)		0 (<5)	0.75	0.32	0.32
66	−0.68±0.10	G		0.9 (0.6–1.7)	1 (<3)	0.30	0.13	0.17
67	0.34±0.01	B	0.51 ^f (0.46–0.56)	0.15 (0.14–0.17)	0 (<1)	240	100	100
68	0.07±0.20	U	1.7 (0.9–3.7)		0.02 (<12)	0.13	0.056	0.056
69	1.00±0.77	M	1.4 (>−0.6)		28 (<910)	0.42	0.18	0.27
70	0.44±0.29	U	0.8 (−0.1–3.4)		0 (<64)	0.15	0.065	0.065
71	−0.09±0.10	R	1.6 (1.3–2.1)		0 (<3)	0.84	0.36	0.36
72	−0.37±0.12	G	3.2 (2.4–4.7)		3 (<11)	0.36	0.16	0.23
73	0.32±0.11	U	1.4 (0.9–2.1)		2 (<11)	0.37	0.16	0.17
74	0.43±0.05	B	0.7 (0.5–0.9)		0.4 (<4)	1.5	0.65	0.65
74		D				1.6	0.69	0.69
74		G				1.7	0.73	0.73
75	0.34±0.32	R	0.4 (−1.1–2.5)		2 (<62)	0.52	0.22	0.23
76	0.19±0.13	D	1.9 (1.2–2.7)		9 (2–19)	0.46	0.20	0.28
76		G				0.36	0.16	0.22
77	0.14±0.39	U	1.4 (0.0–5.4)		3 (<740)	0.12	0.052	0.056
78	0.36±0.06	B	0.8 (0.6–1.0)		0 (<4)	1.3	0.56	0.56
78		D				1.1	0.48	0.48
78		G				0.79	0.34	0.34
79	0.66±0.11	M	2.4 (0.5–4.4)		110 (13–210)	0.67	0.29	1.3

Table 6. (Continued)

No.	HR ^a	Obs. ID ^b	Γ^c	kT^c	N_{H}^c	F_{X}^d	L_{obs}^d	L_{X}^d
80	-0.37±0.13	M	2.6 (2.0–4.4)		0.4 (<9)	0.59	0.25	0.27
81	-0.86±0.01	B		— see Yokogawa et al. (2000e) —		14	6.0	7.3
82	-0.88±0.04	D		1.0 (0.8–1.5)	0 (<0.3)	1.0	0.43	0.43
83	-0.20±0.08	D	2.2 (1.9–2.6)		0 (<2)	0.30	0.13	0.13
84	-0.28±0.12	D	2.6 (2.1–3.5)		0 (<3)	0.16	0.069	0.069
85	...	D
86	0.16±0.11	D	1.3 (0.9–2.0)		0.3 (<8)	0.38	0.16	0.16
87	0.68±0.35	D	4.2 (1.5–9.7)		51 (12–150)	0.19	0.082	1.8
88	...	N
89	...	N
90	0.33±0.003	I	0.79 (0.76–0.82)	0.144 (0.137–0.150)	2.3 (1.6–3.0)	370	160	170
91	0.31±0.26	N	2.0 (>1.0)		2 (<160)	0.11	0.048	0.052
92	-0.08±0.21	N	1.4 (0.6–2.7)		0 (<8)	0.23	0.099	0.099
93	0.36±0.23	N	1.3 (0.6–3.1)		0 (<20)	0.17	0.073	0.073
94	0.43±0.01	A	0.69 (0.61–0.76)	0.13 (0.11–0.15)	4 (2–6)	220	95	110
94	0.40±0.02	C	0.45 (0.35–0.53)	0.20 (0.13–0.29)	0 (<2)	8.9 ^g	3.8 ^g	3.8 ^g
94	0.44±0.01	I	0.35 (0.27–0.44)	0.16 (0.13–0.19)	2 (<4)	150	65	67
95	-0.43±0.09	C	3.3 (2.8–3.9)		0 (<1)	0.38	0.16	0.16
96	-0.36±0.13	V	2.6 (2.0–4.0)		1 (<10)	0.68	0.29	0.34
97	0.24±0.18	V	0.6 (–0.1–1.2)		0 (<12)	0.35	0.15	0.15
98	0.41±0.20	V	1.2 (0.5–2.5)		3 (<21)	0.37	0.16	0.18
99	1.00±0.74	V	5.2 (>1.9)		110 (29–290)	0.44	0.19	31
100	0.11±0.07	V	2.4 (1.8–3.1)		8 (3–16)	0.41	0.18	0.30
101	-0.22±0.18	V	2.1 (1.3–4.3)		1 (<14)	0.45	0.19	0.21
102	0.63±0.17	V	1.9 (0.8–3.6)		24 (5–59)	0.99	0.43	0.78
103	0.18±0.11	O	1.2 (0.9–1.6)		0 (<4)	1.8	0.78	0.78
104	0.20±0.10	O	1.1 (0.8–1.8)		0 (<8)	1.7	0.73	0.73

Table 6. (Continued)

No.	HR ^a	Obs. ID ^b	Γ^c	kT^c	N_{H}^c	F_{X}^d	L_{obs}^d	L_{X}^d
105	-0.06±0.12	O	2.8 (1.7–4.8)		7 (<20)	0.34	0.15	0.29
106	-0.21±0.31	O	6.6 (>1.8)		29 (<88)	0.14	0.060	6.5

a: Hardness ratio and 1- σ error (subsubsection 4.2.2).

b: Observation ID. Flux and luminosity are given for each ID.

c: Photon index Γ , temperature kT (keV), and absorption column density N_{H} (10^{21} cm^{-2}). The parentheses represent 90% confidence limits. For sources showing soft excess (Nos. 67, 90, and 94), a two-component model consisting of a power-law (with exponential cutoff only for No. 67) plus a blackbody was used; thus the temperature in the table is for the blackbody component.

d: Flux F_{X} ($10^{-12} \text{ erg s}^{-1} \text{ cm}^{-2}$), observed luminosity L_{obs} ($10^{36} \text{ erg s}^{-1}$), and absorption-corrected luminosity L_{X} ($10^{36} \text{ erg s}^{-1}$) in 0.7–10 keV.

e: The best-fit model yielded an unusually high luminosity of $\sim 3 \times 10^{39} \text{ erg s}^{-1}$. This is probably an artifact due to the large values of Γ and N_{H} , thus we omitted it from the table.

f: A power-law model with a high-energy cutoff was used. Cut-off and e -fold energies were respectively determined to be 6.4 (5.8–6.9) keV and 6.3 (4.4–9.4) keV.

g: The intrinsic intensity would be much higher (see subsubsection 5.1.22).

Table 7. Luminosities of the long period pulsars in our Galaxy.

Name	Period (s)	Distance (kpc)	L_X (erg s^{-1})	References
X Per	835	0.95 ¹	$< (2 - 10) \times 10^{33}$	1
RX J1037.5–5647	862	5 ²	1×10^{33}	2
SAX J2239.3+616	1247.2	4.4 ³	9×10^{32}	3
RX J0146.9+6121	1404.2	2.5 ⁴	$< (2 - 5) \times 10^{33}$	4
2S 0114+650	10008	7.2 ⁵	6×10^{34}	5

Note. — Luminosities are converted from fluxes presented by Liu et al. (2000), assuming the distances in each reference.

References — (1) Telting et al. (1998); (2) Motch et al. (1997); (3) In 't Zand et al. (2000); (4) Haberl et al. (1998); (5) Reig et al. (1996)

Table 8. Nonpulsating HMXBs and likely candidates in the SMC.

— Number ^a —		Name	Optical ^b	Variable? ^c	Grade ^d	References
ASCA	HRI		identification			
...	1	RX J0032.9–7348	Be ¹	Yes ²	A	1,2
...	22	SMC X-3	Be ³	Yes ⁴	A	3,4
...	...	1H 0103–762	Be ⁵	Yes ²	A	2,5
...	42	RX J0101.0–7206	Be ¹	Yes ²	A	1,2
...	...	EXO 0114.6–7361	B (SG) ⁶	Yes ⁶	A	6
...	24	2E 0051.1–7304	Be ¹	Yes? ⁶	B	1,6
63	38	RX J0058.2–7231	Be ¹	...	B	1
...	...	RX J0106.2–7205	Be ¹	...	B	1
22	...	AX J0048.2–7309	Be? ⁸	Yes ⁸	C	7
50	30	RX J0054.9–7245	Be? ¹	Yes ¹	C	1
...	36	RX J0057.8–7207	Be? ¹	Yes ¹	C	1
...	44	RX J0101.6–7204	Be? ¹	Yes ¹	C	1
76	45	RX J0101.8–7223	Be? ¹	Yes ¹	C	1
...	50	RX J0103.6–7201	Be? ¹	Yes ¹	C	1
...	53	RX J0105.1–7211	Be? ¹	Yes ⁹	C	1,8
87	56	RX J0107.1–7235	Be? ¹	Yes ¹	C	1
...	2	RX J0041.2–7306	Be? ¹	...	D	1
...	3	RX J0045.6–7313	Be? ¹	...	D	1
...	8	RX J0048.5–7302	Be? ¹	...	D	1
28	11	RX J0049.5–7331	Be? ¹	Yes? ⁸	D	1,7
...	14	RX J0050.7–7332	Be? ¹	...	D	1
35	15	RX J0050.9–7310	Be? ¹	...	D	1
...	17	RX J0051.3–7250	Be? ¹	...	D	1
...	21	No. 26 in WW92	Be? ¹	...	D	1
...	26	RX J0053.4–7227	Be? ¹	...	D	1
...	29	RX J0054.5–7228	Be? ¹	...	D	1
...	32	2E 0054.4–7237 (IKT13)	Be? ¹	...	D	1
...	34	2E 0055.8–7229 (IKT15)	Be? ¹	...	D	1
...	37	RX J0057.9–7156	Be? ¹	...	D	1
...	51	RX J0104.1–7243	Be? ¹	...	D	1

Table 8. (Continued)

— Number ^a —		Name	Optical ^b identification	Variable? ^c	Grade ^d	References
ASCA	HRI					
...	52	RX J0104.5–7121 ^e	Be? ¹	...	D	1
...	54	RX J0105.7–7226	Be? ¹	...	D	1
85	55	RX J0105.9–7203	Be? ¹	...	D	1
...	60	RX J0119.6–7330	Be? ¹	...	D	1
...	5	RX J0047.3–7239	Be?AGN? ^{f,1}	...	E	1
...	18	RX J0051.8–7159	Be?AC? ^{g,1}	...	E	1

a: Source number in the catalogues of ASCA (table 5) and HRI (Haberl, Sasaki 2000).

b: Spectral type of the optical counterpart. “Be?” indicates an emission line object catalogued in Meyssonier and Azzopardi (1993) or Murphy and Bessell (2000). “SG” indicates a supergiant counterpart.

c: For sources with the “Yes” sign, long-term X-ray variability has been found.

d: In table 5, we designate grade A and B sources as NH and grade C and D sources as NHc. Grade E sources are not regarded as non-pulsating HMXBs (see subsection 6.2.1).

e: This source is designated as RX J0104.5–7121 in Haberl and Sasaki (2000) (subsection 6.4), but probably should be RX J0104.5–7221 according to its coordinate.

f: A point-like radio source is also located in the error circle, thus the possibility that it is an AGN remains (Haberl, Sasaki 2000).

g: X-ray emission may be attributable to an active corona (AC) of a late type star (Haberl, Sasaki 2000).

References — (1) Haberl and Sasaki (2000); (2) Kahabka and Pietsch (1996); (3) Crampton et al. (1978); (4) Clark et al. (1978); (5) Whitlock and Lochner (1994); (6) Wang and Wu (1992); (7) this work; (8) Filipović et al. (2000b);

Table 9. Source populations in the SMC and in our Galaxy.

	HMXBs			LMXBs	SNRs		
	XBPs	Nonpulse	Candidates		Crab-like	Others	Candidates
Galaxy	53	30	...	130	10	220	100
Galaxy $\times 1/100^a$	0.53	0.3	...	1.3	0.1	2.2	1
SMC	26	8	40	0	0	14	7

a: Since the mass of the SMC is about 1/100 of that of our Galaxy, the source numbers in our Galaxy should be divided by 100 for a simple comparison.